Posted on 1 Jun 2023 — The copyright holder is the author/funder. All rights reserved. No reuse without permission. — https://doi.org/10.22541/essoar.168565382.21382160/v1 — This a preprint and has not been peer reviewed. Data may be preliminary.

Investigating the Impact of Irrigation on Malaria Vector Larval Habitats and Transmission using a Hydrology-based Model

Ai-Ling Jiang[1], Ming-Chieh Lee[2], Prashanth Selvaraj[3], Teshome Degefa[4], Hallelujah Getachew[4], Hailu Merga[5], Delenasaw Yewhalaw[4], Guiyun Yan[2], and Kuo-lin Hsu[6]

[1]Center for Hydrometeorology and Remote Sensing, Department of Civil and Environmental Engineering, University of California Irvine
[2]Department of Population Health and Disease Prevention, School of Public Health, Susan and Henry Samueli College of Health Sciences, University of California Irvine
[3]Institute for Disease Modeling, Bill and Melinda Gates Foundation
[4]School of Medical Laboratory Sciences, Institute of Health, Jimma University
[5]Department of Epidemiology, Institute of Health, Jimma University
[6]University of California, Irvine

June 1, 2023

Abstract

A combination of accelerated population growth and severe droughts have created pressure on food security and driven the development of irrigation schemes across sub-Saharan Africa. Irrigation has been associated with increased malaria risk, but it remains difficult to understand the underlying mechanism and develop countermeasures to mitigate its impact. While investigating transmission dynamics is helpful, malaria models cannot be applied directly in irrigated regions as they typically rely only on rainfall as a source of water to quantify larval habitats. By coupling a hydrologic model with an agent-based malaria model for a sugarcane plantation site in Arjo, Ethiopia, we demonstrated how incorporating hydrologic processes to estimate larval habitats can affect malaria transmission. Using the coupled model, we then examined the impact of an existing irrigation scheme on malaria transmission dynamics. The inclusion of hydrologic processes increased the variability of larval habitat area by around two-fold and resulted in reduction in malaria transmission by 60%. In addition, irrigation increased all habitat types in the dry season by up to 7.4 times. It converted temporary and semi-permanent habitats to permanent habitats during the rainy season, which grew by about 24%. Consequently, malaria transmission was sustained all-year round and intensified during the main transmission season, with the peak shifted forward by around one month. Lastly, we demonstrated how habitat heterogeneity could affect the spatiotemporal dynamics of malaria transmission. These findings could help larval source management by identifying transmission hotspots and prioritizing resources for malaria elimination planning.

Hosted file

964441_0_art_file_11026573_rv9907.docx available at https://authorea.com/users/624016/articles/646515-investigating-the-impact-of-irrigation-on-malaria-vector-larval-habitats-and-transmission-using-a-hydrology-based-model

Investigating the Impact of Irrigation on Malaria Vector Larval Habitats and Transmission using a Hydrology-based Model

Ai-Ling Jiang[1], Ming-Chieh Lee[2], Prashanth Selvaraj[3], Teshome Degefa[4,5], Hallelujah Getachew[4,5,6], Hailu Merga[7], Delenasaw Yewhalaw[4,5], Guiyun Yan[2], Kuolin Hsu[1]

1. Center for Hydrometeorology and Remote Sensing, Department of Civil and Environmental Engineering, University of California Irvine, Irvine, CA, USA
2. Department of Population Health and Disease Prevention, School of Public Health, Susan and Henry Samueli College of Health Sciences, University of California Irvine, Irvine, CA, USA
3. Institute for Disease Modeling, Bill and Melinda Gates Foundation, Seattle, WA, USA
4. School of Medical Laboratory Sciences, Institute of Health, Jimma University, Jimma, Ethiopia
5. Tropical and Infectious Diseases Research Center (TIDRC), Jimma University, Jimma, Ethiopia
6. Department of Medical Laboratory Technology, Arbaminch College of Health Sciences, Arba Minch, Ethiopia
7. Department of Epidemiology, Institute of Health, Jimma University, Jimma, Ethiopia

Corresponding author: Ai-Ling Jiang (jiangal@uci.edu) , Guiyun Yan (guiyuny@uci.edu), Kuolin Hsu (kuolinh@uci.edu)

Key Points:

- An agent-based malaria model was coupled with a hydrologic model to spatially simulate transmission by resolving habitat heterogeneity
- The coupling framework enhanced larval habitat area variability which resulted in a lower malaria transmission prediction
- Irrigation sustained transmission year-round, intensifying and shifting the peak forward by one month from the original period

Abstract

A combination of accelerated population growth and severe droughts have created pressure on food security and driven the development of irrigation schemes across sub-Saharan Africa. Irrigation has been associated with increased malaria risk, but it remains difficult to understand the underlying mechanism and develop countermeasures to mitigate its impact. While investigating transmission dynamics is helpful, malaria models cannot be applied directly in irrigated regions as they typically rely only on rainfall as a source of water to quantify larval habitats. By coupling a hydrologic model with an agent-based malaria model for a sugarcane plantation site in Arjo, Ethiopia, we demonstrated how incorporating hydrologic processes to estimate larval habitats can affect malaria transmission. Using the coupled model, we then examined the impact of an existing irrigation scheme on malaria transmission dynamics. The inclusion of hydrologic processes increased the variability of larval habitat area by around two-fold and resulted in reduction in malaria transmission by 60%. In addition, irrigation increased all habitat types in the dry season by up to 7.4 times. It converted temporary and semi-permanent habitats to permanent habitats during the rainy season, which grew by about 24%. Consequently, malaria transmission was sustained all-year round and intensified during the main transmission season, with the peak shifted forward by around one month. Lastly, we demonstrated how habitat heterogeneity could affect the spatiotemporal dynamics of malaria transmission. These findings could help larval source management by identifying transmission hotspots and prioritizing resources for malaria elimination planning.

Plain Language Summary

Population growth and severe droughts have driven the development of irrigation schemes across sub-Saharan Africa, which can increase malaria risk. The relationship between irrigation and malaria transmission dynamics remains unclear. Malaria models are seldom used to investigate this relationship as they typically rely only on rainfall to quantify larval habitats. By coupling a hydrologic model with a malaria model for a sugarcane plantation site in Arjo, Ethiopia, we demonstrated how incorporating hydrologic processes to estimate larval habitats can affect malaria transmission. Using the coupled model, we then examined the impact of the local irrigation on malaria transmission. The inclusion of hydrologic processes increased the variability of larval habitat area and resulted in a significant reduction in malaria transmission. In addition, irrigation increased all habitat types in the dry season and prolonged habitat stability during the rainy season. Consequently, malaria transmission was sustained year round and intensified during the main transmission season, with the peak shifted forward by around one month. Lastly, we demonstrated how habitat distribution could affect the spatiotemporal dynamics of malaria transmission. These findings could help identify mosquito breeding hotspots and prioritize resources for malaria elimination planning.

1. Introduction

Malaria is a deadly disease caused by parasites transmitted to humans through the bites of infected female *Anopheles* mosquitoes. It is particularly acute in sub-Saharan Africa and remains one of the region's most pressing public health challenges. About 95% of malaria cases and 96% of deaths in 2020 were recorded in sub-Saharan Africa (World Health Organization, 2021). A combination of accelerated population growth and arid conditions worsened by climate change has inevitably created pressure on food security (Ward et al., 2016). This drives the development of several regional irrigation schemes, which have been associated with increased malaria risk (Mangani et al., 2022). In past studies, the association has been chiefly demonstrated by statistical relationships based on field observations (Haileselassie et al., 2021; Kibret et al., 2014; Ondeto et al., 2022). However, these relationships may only be represented in some environmental settings because field observations are made at a limited number of discrete points in space and time.

Malaria modeling has the potential to complement field studies by exploring hypothetical scenarios and making a priori predictions that can inform intervention strategies. Originating from the basic Ross-Macdonald model (Ross, 1908), many compartmental models have inherited its simplifying assumptions, such as homogeneous biting and well-mixing of hosts and vectors, which is a shortcoming of representing the vectors and hosts as a population group rather than individuals (Reiner et al., 2013). In cases where spatial heterogeneity and stochasticity of disease progression are essential such as in a low-transmission setting, agent-based models (ABMs) can provide an explicit representation of individual actions and responses (N. R. Smith et al., 2018). Examples of advanced ABMs include Epidemiological MODeling (EMOD) (P. A. Eckhoff, 2011), OpenMalaria (T. Smith et al., 2006), and a model developed at Imperial College (Griffin et al., 2010). While widely used in malaria intervention studies (Galactionova et al., 2021), these models tend to neglect the larval habitat representation (Griffin et al., 2010; T. Smith et al., 2006) or rely only on rainfall to quantify larval habitats (P. A. Eckhoff, 2011).

A recent study by Smith et al. demonstrated that using a hydrologic model to simulate habitat availability can uncover more complex patterns in climatic suitability for malaria transmission than applying a rainfall threshold (M. W. Smith et al., 2020). This is because the formation of larval habitats is heavily influenced by hydrologic processes, which are highly non-linear and spatially variable. In a hydrologic cycle, rainfall is partitioned into infiltration and surface runoff based on the soil type. Depending on the topography and surrounding vegetation, the resulting surface runoff will accumulate or drain. The persistence of the ponded water can also be influenced by evapotranspiration which varies with land use type. Besides rainfall, breeding sites can develop from groundwater, irrigation, reservoirs, and around dams. In irrigated settings, irrigation varies seasonally with crop production. Within a season, irrigation changes with local soil saturation and crop water use. The spatiotemporal variability of irrigation can result in habitats with different persistence and productivity. This diversity in habitat characteristics complicates the pattern of adult mosquito density and malaria transmission intensity (Frake et al., 2020; Hardy et al., 2013; Munga et al., 2006). Therefore, incorporating hydrologic processes into malaria modeling to capture habitat heterogeneity is essential and can help provide better insights into how irrigation affects malaria transmission.

There have been attempts to represent surface hydrology in malaria transmission modeling with varying levels of complexity and success (Ernest O. Asare et al., 2016). Most resort to a simple conceptual water balance model to determine the availability of water for

larval habitats (Ernest Ohene Asare et al., 2016; Montosi et al., 2012; Parham et al., 2012; Patz et al., 1998), while only a few have proposed more sophisticated hydrologic models that further consider canopy processes and subsurface flows (Bomblies et al., 2008; Le et al., 2018). Despite representing larval habitats more realistically, their malaria transmission component is often less comprehensive than advanced ABMs. Furthermore, none of these studies have investigated the impact of irrigation on malaria transmission.

In this study, we integrate a physical-based hydrologic model, ParFlow-Community Land Model (ParFlow-CLM) (Ashby & Falgout, 1996; Jones & Woodward, 2001; Kollet & Maxwell, 2006; Maxwell, 2013; Maxwell & Kollet, 2008), with EMOD for a test site in Ethiopia. We chose EMOD because it is open-source and can be easily modified to assimilate inputs from an external hydrologic model. We aim to demonstrate how incorporating hydrologic processes to estimate larval habitats can affect malaria transmission intensity and seasonality. Using the coupled model, we then examine the impact of an existing irrigation scheme on the spatiotemporal dynamics of malaria transmission.

2. Materials and Methods

2.1. Study Site

We conducted this study in the Arjo-Didessa sugarcane plantation and its vicinity in the Didessa river valley, near Arjo town in Oromia Regional State, western Ethiopia (Figure 1). The study site includes a commercial sugar factory and an active irrigation area that relies on seasonal migrant workers for planting and harvesting. The site elevation ranges from 1,275 to 2,105 m above sea level, with a mean annual rainfall of 1,560 mm from 1994 to 2020 (Figure S1). The primary rainy season is between May and October, and the dry season occurs for the rest of the year. Monthly average relative humidity varies widely from around 40% to 80%. It follows the rainfall pattern, while the monthly average temperature ranges from 19 °C to 24 °C and is lower in the rainy season than in the dry season (Figure S2). Flow and sprinkler irrigation are commonly practiced on the plantation (Fikadu, 2015). Due to poor drainage caused by the low permeability of the extensive heavy clay, the area is a perennial hotspot for larval habitats and is known to be malarious (Demissew et al., 2020; Hawaria et al., 2019). Malaria prevalence in this area is less than 3%, and transmission is seasonal, with cases peaking between September to December (Hawaria et al., 2019). *Anopheles arabiensis* is the primary malaria vector in this area. Local clinical malaria data shows that both major malaria parasites in Ethiopia, *Plasmodium falciparum* and *Plasmodium vivax,* co-exist with equal incidences but significant seasonality (Hawaria et al., 2019).

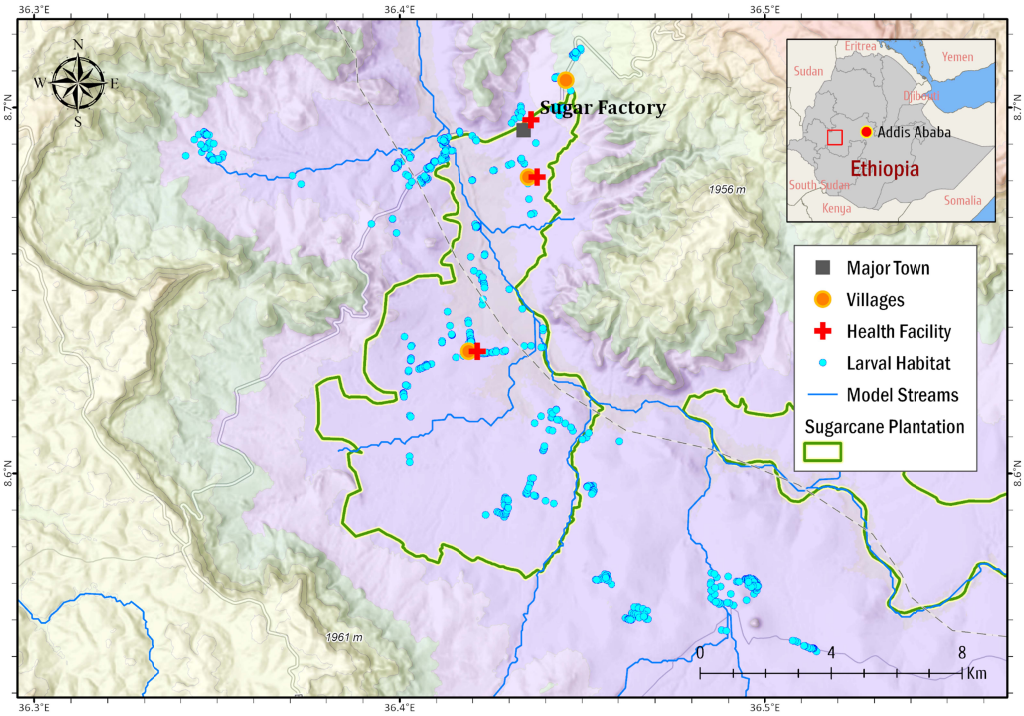

Figure 1. Arjo-Dedissa study site. The sugarcane plantation is demarcated in green within the study site. The surveyed larval habitats, represented by the blue markers, were used to estimate larval density and calibrate the hydrologic model. The three red crosses represent health facilities frequented by plantation workers from nearby villages and provide clinical data for EMOD calibration.

2.2. Data Collection

ParFlow-CLM requires climate data, including rainfall, short-wave radiation, long-wave radiation, air temperature, surface pressure, specific humidity, and wind speeds, to drive the hydrologic processes. The data were obtained from Precipitation Estimation from Remotely Sensed Information using Artificial Neural Networks-Cloud Classification System-Climate Data Record (PERSIANN-CCS-CDR) (Sadeghi et al., 2021) and the Fifth Generation European Centre for Medium-Range Weather Forecasts Reanalysis (ERA5) (Hersbach et al., 2018). Air temperature, humidity, and long-wave radiation were adjusted to account for the mismatch in surface elevation between ERA5 and the study area, following the method by Cosgrove et al. (2003). For processes at the land surface, topography was obtained from a commercial global digital elevation model, ALOS World 3D (Takaku & Tadono, 2017) with additional hydro-conditioning (Jiang et al., 2023), and land cover information was extracted from Global Land Cover Mapping Project, which is based on Landsat and Chinese HJ-1 satellite images (Chen et al., 2015). To characterize the subsurface, soil properties were referenced from the SoilGrids250m TAXOUSDA dataset (Hengl et al., 2017) for the top 2 m from the surface, and the parameters for the deeper geological layer beyond the top 2 m were defined using GLHYMPS 2.0 (Gleeson et al., 2014). The bottom of the geological layer was delineated based on the depth to bedrock data from SoilGrids250m (Hengl et al., 2017). The climate inputs for EMOD include rainfall, air temperature, land temperature, and humidity. The rainfall data were

similarly obtained from PERSIANN-CCS-CDR, and the others were extracted from ERA5. The list of model input data can be found in Table S1.

Besides publicly available data, several field surveys were conducted to support model development (Table S2). In previous studies, larval habitat data were collected over seasonal campaigns from 2017 to 2021, with a total of 769 sampled points (Hawaria et al., 2020). The larval habitat survey was conducted within 500 meters of the village boundaries and sugarcane plantations. The surveyed larval habitat locations are shown in Figure 1. Mosquito larvae were sampled following the World Health Organization (WHO) standard larval survey procedure using a standard dipper (350 ml). Larvae were identified morphologically and sorted by genus as *Anopheles* or *Culex* in the field. From the survey, habitat locations within the hydrologic modeling domain were used to validate the predicted aquatic habitats simulated in ParFlow-CLM, and larval density was used to determine the larval carrying capacity of the habitats in EMOD. In addition to the larval habitat survey, a land cover field survey was conducted in July 2021 in the study area. The survey was performed every 400 meters along the perpendicular transects, spaced every 2 km apart along each of the 12 major road segments, with a total of 400 survey points (Figure S3). Survey results were collected with Open Data Kit (Hartung et al., 2010) and used to validate satellite imagery. The most common land cover type in the study area was cropland and natural vegetation mosaics (Figure S4).

To configure the parameters in EMOD and validate the model, population data, malaria incidence, and parasite prevalence rates were collected from previous works. Population data were obtained from demographic surveys in the sugar factory command village and vicinity communities from 2018 to 2021. Clinical cases for the 2008 to 2017 period were referenced from the malaria morbidity registration books (Hawaria et al., 2019). The prevalence rate was calculated based on passive case detection implemented at the Arjo Sugar Factory Clinic and two other health facilities in 2018 and 2019. Since there were no official records of malaria control campaigns in the study area for the past 20 years, we also interviewed the district health officers, clinical staff in health facilities, and sugar factory administrations to estimate the coverage, duration, and the total number of long-lasting insecticidal bed nets (LLIN) distributed and indoor residual spraying (IRS) applied (personal communication, April 30, 2022).

2.3. Model Approach

2.3.1. Model Background

We used ParFlow-CLM, a process-based gridded model, to simulate hydrologic processes in the Arjo study site in Ethiopia. ParFlow solves the variably saturated subsurface flow and overland flow, while CLM calculates the canopy water balance and terrestrial energy balance, which are influenced by land cover characteristics. Due to its ability to simulate complex surface-subsurface interactions, ParFlow-CLM can resolve a diverse range of water bodies driven by heterogenous hydrological and geomorphological processes, which result in different breeding habitats such as rain-fed pools, flood basins, and spring-fed ponds (M. W. Smith et al., 2013).

EMOD was used to simulate malaria transmission in the study area. The modeled region in EMOD can be represented as a single node or divided into multiple nodes. As a stochastic ABM, it simulates the simultaneous interactions between humans and mosquitoes within each node, using decision rules based on individual agent properties with inbuilt randomness (Bill &

Melinda Gates Foundation, 2022). The properties are defined by user inputs on demographic, climate, mosquito, parasite, and intervention parameters. The model simulates vector population dynamics (e.g., vector life cycle, vector survival and feeding), human population dynamics, human immunity, within-host parasite dynamics, and effects of interventions such as antimalarial drugs and vaccines (P. Eckhoff, 2013).

2.3.2. Linking Habitat Representation in EMOD with ParFlow-CLM

In EMOD, natural larval habitats commonly comprise temporary, semi-permanent and permanent (constant) habitats, and each habitat type is calculated based on a different equation (P. A. Eckhoff, 2011). Temporary habitats are driven mainly by rainfall and decay at a rate proportional to the evaporation rate, which is a function of temperature and humidity. The area of temporary habitats in each node at time t, H_{temp}^{t}, is calculated by:

$$H_{temp}^{t} = H_{temp}^{t-1} + \lambda_{temp} P^{t} {D_{cell}}^{2} - H_{temp}^{t-1} \tau_{temp}^{t} \Delta t \tag{1}$$

and

$$\tau_{temp}^{t} = 5.1 \times 10^{11} e^{\frac{-5628.1}{T^{t}}} k_{temp} \sqrt{\frac{0.018}{2\pi R T^{t}}} (1 - RH^{t}) \ , \tag{2}$$

where λ_{temp} is a scaling factor, P^{t} is rainfall at time t, τ_{temp}^{t} is a decay rate at time t, D_{cell} is the nodal size in degree, Δt is the time interval, T^{t} is the temperature in Kelvin at time t, k_{temp} is a decay factor, R is the universal gas constant 8.314 J/mol/K and RH^{t} is the relative humidity at time t.

Similar to temporary habitats, semi-permanent habitats are also driven by rainfall, but the decay rate is a constant that is independent of temperature and humidity. Semi-permanent habitats are configured to decay slower than temporary habitats. Using a scaling factor λ_{semi} and a decay rate τ_{semi}, the area of semi-permanent habitats H_{semi}^{t} is calculated as:

$$H_{semi}^{t} = H_{semi}^{t-1} + \lambda_{semi} P^{t} {D_{cell}}^{2} - H_{semi}^{t-1} \tau_{semi} \Delta t \ , \tag{3}$$

Lastly, permanent habitats are assumed to be independent of rainfall, temperature, and humidity. The area, H_{perm}^{t}, remains the same over time and is determined by a constant λ_{perm}:

$$H_{perm}^{t} = \lambda_{perm} {D_{cell}}^{2}, \tag{4}$$

As shown in Figure 2, EMOD conceptually models each habitat type within a node as a lumped habitat which is oversimplified and does not have the granularity to support habitat-based interventions. To enhance the fidelity of the model in representing habitats which are spatially distributed in reality, we simulated the habitats explicitly in ParFlow-CLM in place of the default habitat calculation in EMOD.

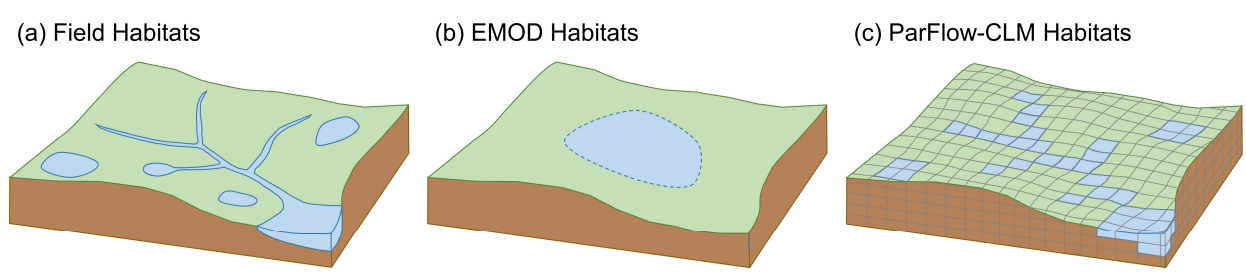

Figure 2. Illustration of (a) field habitats within a study area (b) conceptually lumped habitat calculated in EMOD within a node representing the same study area (c) spatially distributed habitats simulated in Parflow-CLM within the same node.

ParFlow-CLM generated the spatiotemporal distribution of surface soil saturation, which was used to determine the availability of surface water that could contribute to ponding. For each grid cell in ParFlow-CLM, ponding was assumed to occur if the soil saturation exceeds a threshold, θ, which was calibrated based on larval habitat observations. The duration of ponding was quantified and referred to as the Wetness Index. Based on the Wetness Index, each cell was classified into temporary (15-90 days), semi-permanent (90-180 days) or permanent habitat (more than 180 days). Rivers with high flow rates were not considered since *Anopheles* larvae have a lower chance of surviving in fast-moving water (Hardy et al., 2013). Details of the concept of hydrologic simulation and larval habitat identification can be found in Jiang et al. (2021). For each time step, the fraction of the study area covered by each habitat type (i.e., F_{temp}^{t}, F_{semi}^{t}, and F_{perm}^{t}) was calculated and input into EMOD. Finally, the area for each habitat type in each node was obtained after multiplying the fractional area coverage by the nodal area as follows:

$$H_{temp}^{t} = F_{temp}^{t} {D_{cell}}^{2}, \tag{5}$$

$$H_{semi}^{t} = F_{semi}^{t} {D_{cell}}^{2}, \tag{6}$$

and

$$H_{perm}^{t} = F_{perm}^{t} {D_{cell}}^{2}, \tag{7}$$

where F_{temp}^{t}, F_{semi}^{t}, F_{perm}^{t} are the fractional area coverage of temporary, semi-permanent, and permanent habitats, respectively.

2.3.3. Habitat Larval Capacity

EMOD requires the user to define a larval capacity per unit area (LC) for each habitat type, representing the maximum hypothetical number of larvae that can co-exist within a 1-degree by 1-degree habitat area. LC was then multiplied by the nodal time series habitat area in degree^2 (Section 2.3.2). Finally, the variation in larval capacity within a node is defined.

In this study, LC was estimated using field survey data for each habitat type (Text S1). In Table 1, LD_{dip} represents the larval density in number of larvae per dip. We then converted LD_{dip} to an equivalent number of larvae per unit degree squared, LD, based on the opening area of the standard 350 ml mosquito larvae dipper, which is 13 cm in diameter (Orondo et al., 2023). To obtain LC, we adjusted LD by a scaling factor, s, during the calibration of EMOD. The adjustment is necessary because using LD directly will overestimate the larval capacity as surveyors tend to dip at locations with a higher density of larvae within a sampled habitat.

Table 1. Laval density derived from field survey and calibrated larval capacity per unit area for each habitat type.

Habitat Type	Larval Density		Larval Capacity per Unit Area
	LD_{dip} (#/dip)	LD (#/degree^2)	$LC = s \times LD$ (#/degree^2)

Temporary	0.167	1.97×10^{11}	3.27×10^{6}
Semi-Permanent	0.089	1.05×10^{11}	1.74×10^{6}
Permanent	0.440	5.18×10^{11}	8.62×10^{6}

In summary, we identified potential larval habitats in ParFlow-CLM and classified them into temporary, semi-permanent, and permanent habitats as an input to the vector cycle simulation in EMOD. The overall schematic of our modeling approach is shown in Figure 3.

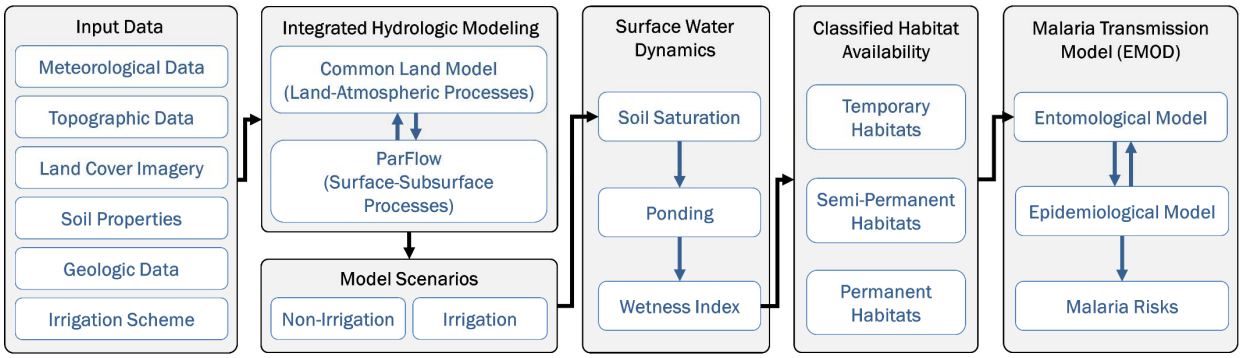

Figure 3. Framework for integrating ParFlow-CLM with EMOD.

2.4. Model Configuration

2.4.1. Model Domain

In a previous study, ParFlow-CLM was successfully applied in Arjo for larval habitat identification over one year through 2018 (Jiang et al., 2021). Here, we expanded the hydrologic simulation to 20 years from 2000 to 2020. The model domain area was 208 km^2 (Figure 1). To keep the computational time manageable, we decreased the spatial resolution from 50 m to 100 m and reduced the number of subsurface layers from 10 to 5 layers. The thickness of the layer from ground surface to bedrock was 0.1 m, 0.3 m, 0.6 m, 1 m, and 78 m, over a total vertical depth of 80 m.

For malaria transmission modeling in EMOD, we focused on the sugarcane plantation area within the hydrologic modeling domain (Figure 1). The EMOD domain was configured as a single node measuring 10 km by 10 km.

2.4.2. Model Scenarios

Three model scenarios were developed for this study. In the first scenario (*Default EMOD*), malaria transmission was simulated based on the default larval habitat equations in EMOD (Equations (1) to (4)). In the second scenario (*Integrated EMOD or Non-Irrigation*), the default larval habitat equations were replaced by the simulated habitats from ParFlow-CLM through Equations (5) to (7), which integrates terrestrial hydrological processes. To investigate the effect of irrigation, a third scenario (*Irrigation*) was added using the same integrated approach from the second scenario, but irrigation was modeled in ParFlow-CLM per the local schedule as described below.

Irrigation was applied starting in 2012, and a 4-year sugarcane planting cycle was adopted in the model, as shown in Figure 4. The cycle includes a 2-year cycle for virgins and two

1-year cycles for ratoons, typical of the sugarcane plantation. The irrigation scheme was designed based on the sugarcane planting cycle, and the months with irrigation are shown in Figure S6. During the irrigating season, irrigation occurred every 10 days for the first 3 days. Daily 5.3 mm/hr of sprinkler water was applied for 22 hours. The derivation of the irrigation rate can be found in Text S2.

In the three scenarios, malaria interventions, including IRS and bed net distribution, were modeled per the schedule shown in Figure 4.

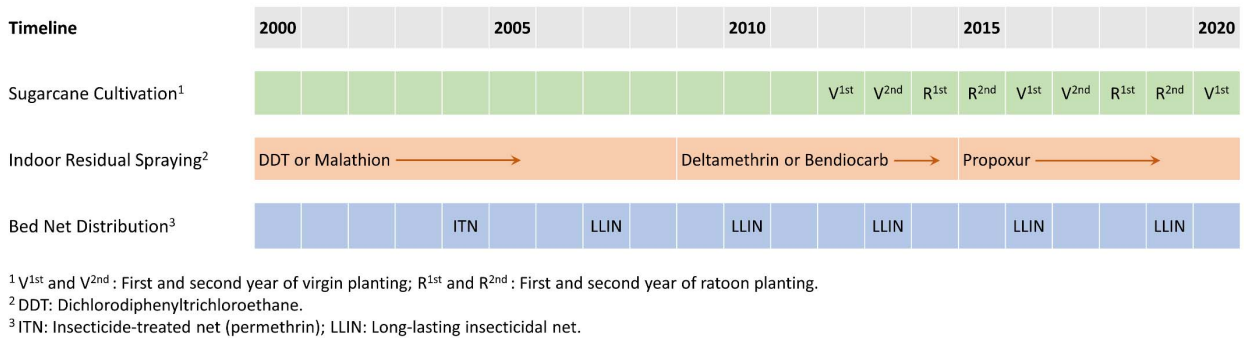

[1] V^{1st} and V^{2nd} : First and second year of virgin planting; R^{1st} and R^{2nd} : First and second year of ratoon planting.
[2] DDT: Dichlorodiphenyltrichloroethane.
[3] ITN: Insecticide-treated net (permethrin); LLIN: Long-lasting insecticidal net.

Figure 4. Configuration of intervention and sugarcane cultivating plan in the integrated model. The irrigation schedule can be referred to in Text S2 and Figure S6.

As it is challenging to ascertain the total area of the habitats in the study area, the scaling factors (λ_{temp}, λ_{semi} and λ_{perm}) in *Default EMOD* were set individually such that the average area of each habitat type over the simulation period was the same as *Integrated EMOD* to allow a fair comparison. In addition, the decay parameters k_{temp} and τ_{semi} in *Default EMOD* were also adjusted to match the variability in *Integrated EMOD* (Figure S7).

2.4.3. Model Calibration

We calibrated ParFlow-CLM and EMOD in the *Irrigation* scenario and used the same calibrated parameters in the *Default EMOD* and *Integrated EMOD* scenarios. This is because observed data was only available for the period after irrigation was implemented in the study area. This also prevented the effect of incorporating hydrologic modeling or irrigation from being obscured by using different parameters in each scenario.

As the spatial resolution in ParFlow-CLM was modified from the previous study (Jiang et al., 2021), we recalibrated the saturation threshold, θ. The calibration was to ensure that the model will predict the occurrence of ponding at locations in line with the field surveyed larval habitats for soil saturation above the selected threshold (Text S3 and Jiang et al., 2021). For the calibration of EMOD, we identified 15 key parameters (Table S3) after a preliminary sensitivity analysis. The calibration aimed to align the simulated prevalence rate and pattern of clinical cases with local data (Text S3). The rest of the parameters were either referenced from published studies (Gerardin et al., 2015; Selvaraj et al., 2018) or set based on default values in EMOD.

2.4.4. Spatial Realization of Transmission through Heterogeneity of Habitats

To demonstrate how the heterogeneity of habitats can affect malaria transmission, we conducted an additional analysis by discretizing the study site into 100 nodes measuring 1 km by 1 km in EMOD. All the nodes were assigned the same calibrated parameters, but the input

habitat was specific to the area covered by each node. This was only applicable to the scenarios with ParFlow-CLM integrated into EMOD. The habitat simulation in *Default EMOD* could not reflect spatial heterogeneity since it cannot process the effects of topography, soil and land cover.

3. Results

3.1. Effect of Hydrology on Larval Habitats and Malaria Transmission

A comparison of the larval habitat area as a fraction of the study area between *Default EMOD* and *Integrated EMOD* is illustrated in Figure 5. In both scenarios, the total larval habitat area varied in tandem with seasonal rainfall, with a mean of 27% (Figure 5a). However, the habitats in *Integrated EMOD* exhibited less frequent daily fluctuations, and its seasonal range was more extensive than *Default EMOD*. Figure 5b shows a violin plot of the average total habitats for each day within a year (intra-annual distribution). In contrast, Figure 5c shows a violin plot of the annual average total habitats (inter-annual distribution) throughout the simulation period. The habitats in *Integrated EMOD* were found to have a more significant intra-annual and inter-annual variability as the standard deviation of the habitats is about 1.8 times and 2 times that of *Default EMOD,* respectively. The reason is attributable to the simplifying assumptions built into the habitat functions in *Default EMOD* and will be discussed further in Section 4.1.

Figure 5d, Figure 5e, and Figure 5f present the breakdown for each habitat type. Of the total larval habitat area, permanent habitats were the most dominant, accounting for 16% of the study area, followed by semi-permanent habitats (8.4%) and temporary habitats (3.3%). In *Integrated EMOD*, the fluctuation in habitat area gradually becomes smoother from temporary to semi-permanent and finally permanent habitats, corresponding with the increasing stability of the habitats. In each year, the distribution between the habitat types can vary significantly depending on the magnitude and duration of rainfall in that year. For example, there were more temporary habitats relative to semi-permanent habitats in 2012 and vice-versa in 2015 due to a difference in rainfall patterns.

In contrast, the difference in stability and dynamic distribution between temporary and semi-permanent habitats was less apparent in *Default EMOD*. Notably, the area of permanent habitats remained constant throughout the years. This is a key difference from *Integrated EMOD*, in which permanent habitats were defined as habitats with more than 180 days of ponding and subject to temporal variations.

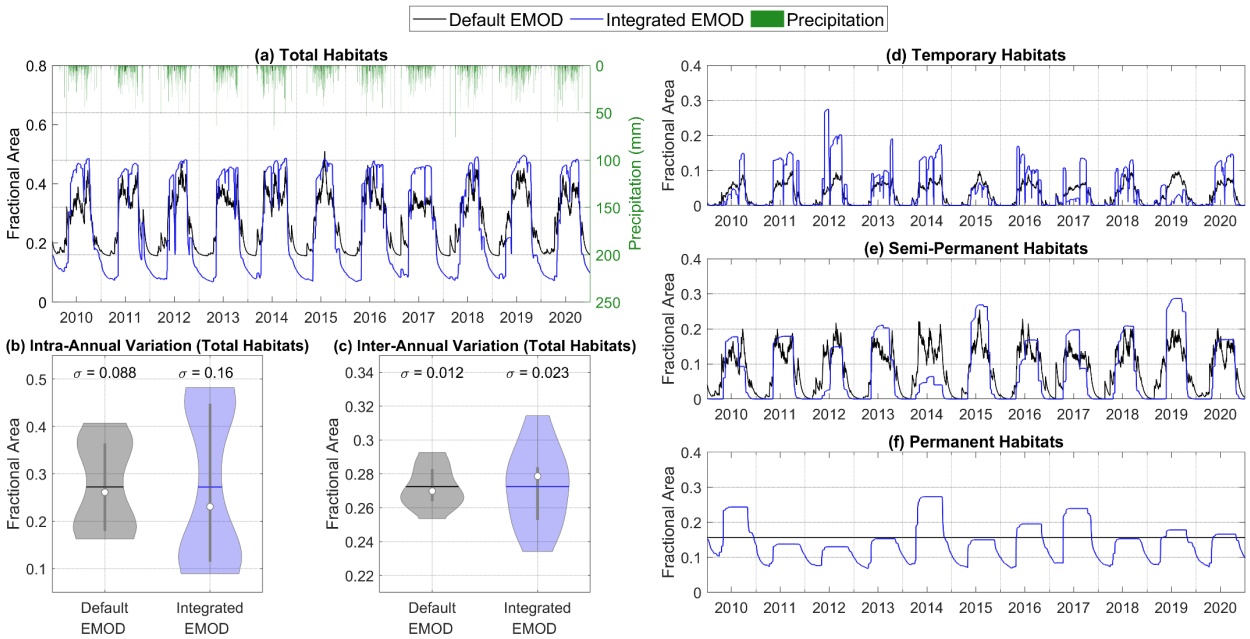

Figure 5. Comparison of daily simulated larval habitat area between *Default EMOD* and *Integrated EMOD* from 2010 to 2020. The simulation was performed for 20 years from 2000 to 2020, but here we only show the results from 2010 to 2020 for simplicity. (a) The total habitat area is broken down into (d) temporary habitats, (e) semi-permanent habitats and (f) permanent habitats. Violin plots were used to illustrate the (b) intra-annual distribution and (c) inter-annual distribution of the total habitat area. Intra-annual distribution is based on the 20-year average habitat area for each day of a year, while inter-annual distribution is characterized by the annual average habitat area for each year. In the violin plots, the white dot and horizontal line represent the median and mean, respectively. The vertical bar in the center of the violin plot corresponds to the interquartile range.

Since the average total larval habitat area was the same in *Default EMOD* and *Integrated EMOD*, the average habitat larval capacity was identical in both scenarios (Figure 6a). However, the number of adult vectors was slightly higher (by 3%) in the "Default EMOD" scenario (Figure 6b). The resulting difference was further amplified to 2.9 times for the average vector infection rate (Figure 6c) and 2.5 times for the average prevalence rate (Figure 6d). Given that all other input data and parameters in EMOD were the same, this can be attributed to the visibly lower variability in the daily habitat larval capacity of *Default EMOD* (Figure S11c), providing a stable environment for the vector to thrive throughout the year. The lower variability in habitat larval capacity is not only due to lower variability in larval habitat area but also the high larval capacity per unit area of permanent habitats whose area does not vary. In summary, the results suggest that incorporating hydrologic modeling can produce higher variability in larval habitat, resulting in lower simulated malaria transmission.

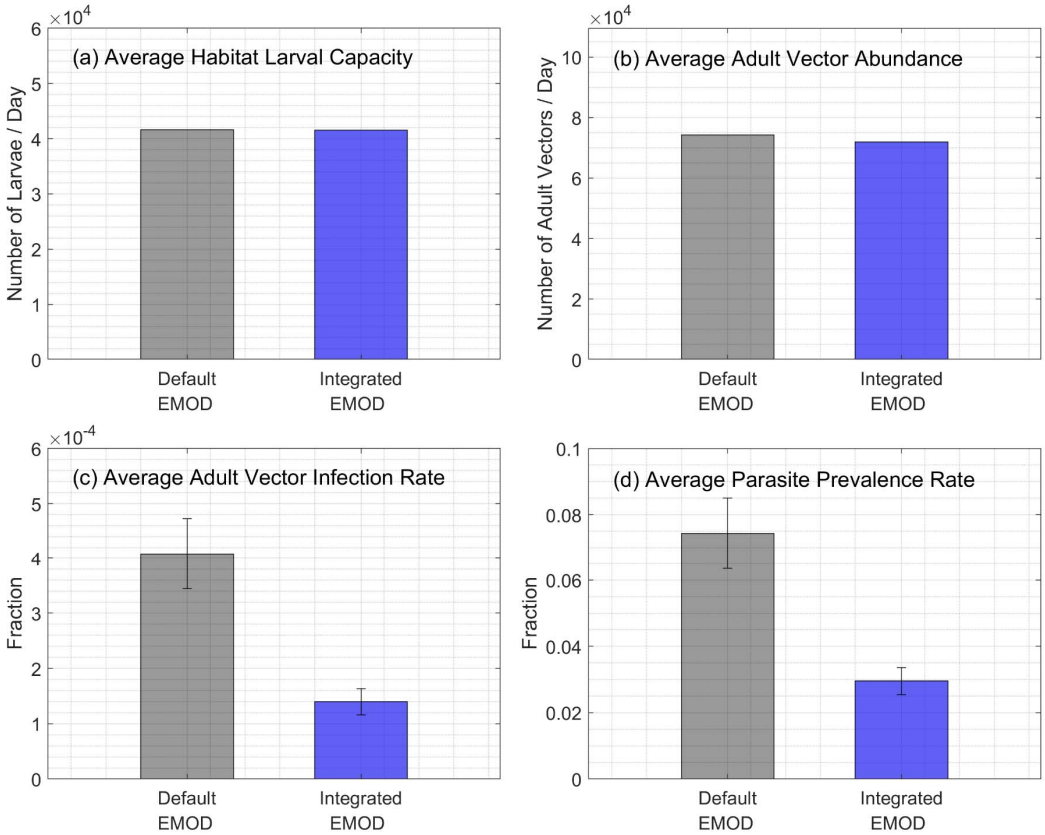

Figure 6. Comparison of annual average malaria transmission indicators between *Default EMOD* and *Integrated EMOD* from 2000 to 2020. The indicators include (a) habitat larval capacity, (b) adult vector abundance, (c) adult vector infection rate, and (d) parasite prevalence rate.

3.2.Effect of Irrigation on Larval Habitats and Malaria Transmission

Irrigation generally increased the habitat area in both dry and rainy seasons. In the dry season (Figure 7a), the increase in median fractional area was the highest for temporary habitats (7.4 times), followed by semi-permanent habitats (6.6 times) and permanent habitats (1.3 times). Although irrigation was only applied in the dry season, it prolonged the stability of temporary and semi-permanent habitats and converted them to permanent habitats in the rainy season (Figure 7b). Temporary and semi-permanent habitats decreased in coverage by about 7% and 8%, whereas permanent habitats grew by 24%. From the results, habitats arising from irrigation may enable the development of vectors in the dry season while stabilizing the growth in rainy seasons.

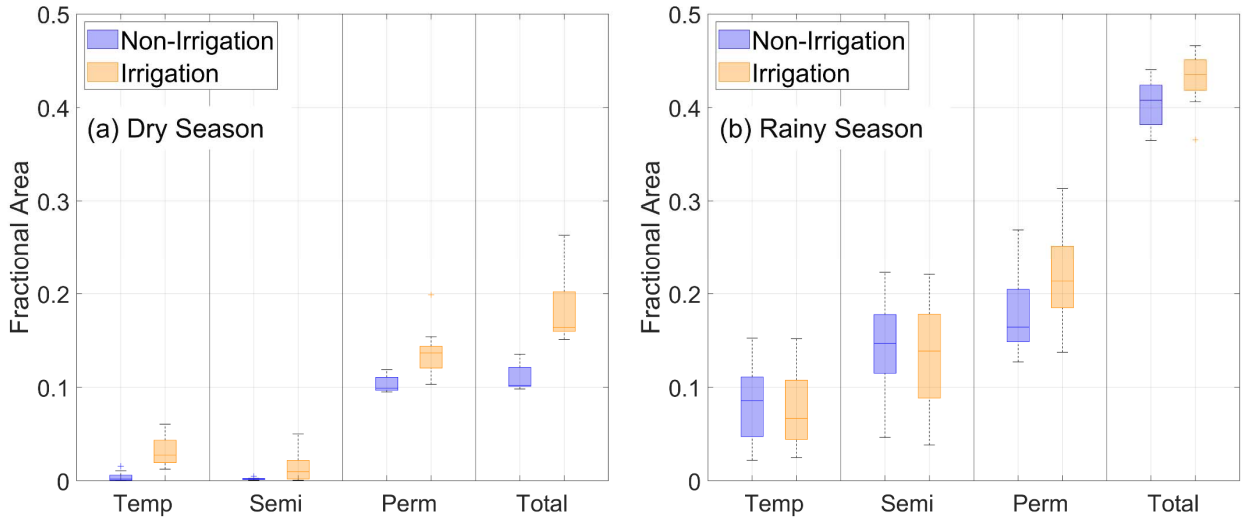

Figure 7. Comparison of larval habitat area during (a) dry season and (b) rainy season from 2012 to 2020 between *Non-Irrigation* and *Irrigation*. Habitats are further classified into temporary, semi-permanent, and permanent types. The horizontal line inside the box represents the median, and the height of the box corresponds to the interquartile range.

Next, we presented the simulated times series of habitat area, larval capacity, adult vector population, entomological inoculation rate (EIR), and parasite prevalence for *Non-Irrigation* and *Irrigation* over the irrigated period in Figure 8. Comparing Figure 8b and Figure 8c, the differences in the larval capacity per unit area for each habitat type introduce more inter-annual variability to larval capacity as the relative abundance of each habitat type is dynamic. The adult vector population's pattern generally follows habitat larval capacity. However, the EIR cycle lags the adult vector population cycle by 2 months, and the parasite prevalence cycle lags the EIR cycle by another 1 month.

The increase in habitat area arising from the applied irrigation contributed to an increase in adult vector population beyond the irrigation periods as well as EIR and parasite prevalence. The simulated daily EIR hit a maximum of 0.0029 in September 2017, a 3-fold increase compared to *Non-Irrigation*, due to the longest preceding irrigation period. In the same year, the maximum prevalence occurred in October, with a 1.9-fold increase to 0.0509. It was also found that the EIR and prevalence peaks, which occurred around October/November and November/December, respectively, were shifted forward by about one month after irrigation was applied.

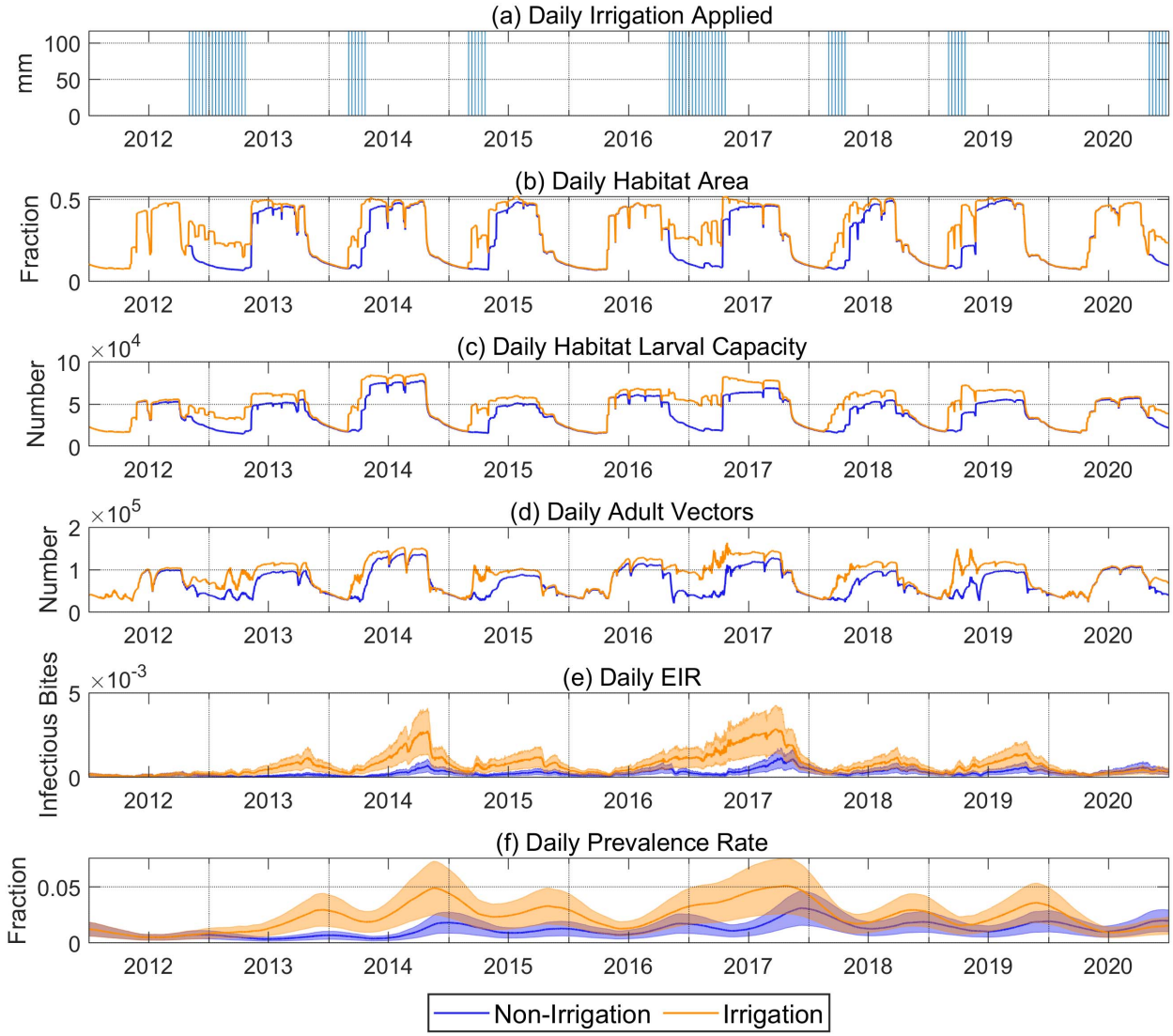

Figure 8. Time series of daily applied irrigation in *Irrigation* and comparison of simulated daily malaria transmission results between *Non-Irrigation* and *Irrigation*. Malaria transmission results include (b) habitat area, (c) habitat larval capacity, (d) adult vector abundance, (e) entomological inoculation rate, and (f) parasite prevalence rate. The simulation was performed for 20 years from 2000 to 2020, but here we only show the results from 2012 onwards, when irrigation began.

3.3. Spatial Variation of Malaria Transmission

The effect of the spatial distribution of larval habitats on malaria transmission is illustrated in Figure 9. Larval habitats formed more easily in the southwestern region (Figure 9a-d) which is characterized by clay-rich soil with low permeability (Figure S12). Besides soil type, the distribution of the habitat types within the study area varied substantially with hydrologic processes depending on the local topography, land use, and irrigation. In both dry and rainy seasons, irrigation expanded the area covered by habitats and increased the stability of existing habitats.

Like habitat areas, the adult vector hotspots in both seasons were enlarged and intensified by irrigation (Figure 9e-h). The increase in vector population was more significant in the dry

season (Table S4) due to the creation of more habitats by irrigation. The adult vector hotspots were mainly concentrated around permanent habitats configured with the highest larval capacity based on field data.

In general, irrigation increased the prevalence rate difference between the rainy and dry seasons. Without irrigation, the parasite prevalence cycle peaked shortly after the rainy season in November and December, which are considered part of the dry season (Figure 8d and Figure 8f). Due to the time lag, although the adult vector population was higher in the rainy season than the dry season, this difference became less apparent when comparing the prevalence rates between the two seasons (Figure 9i and Figure 9k). In 2017, irrigation was applied from November 2016 to April 2017, connecting two rainy seasons and creating favorable conditions for breeding over more than a year (Figure 8c). As a result, the prevalence in the second rainy season from May 2017 to October 2017 (Figure 9l) was visibly higher than the preceding dry season (Figure 9j). This indicates that irrigation can introduce a compounding effect on malaria transmission and alter its seasonal distribution.

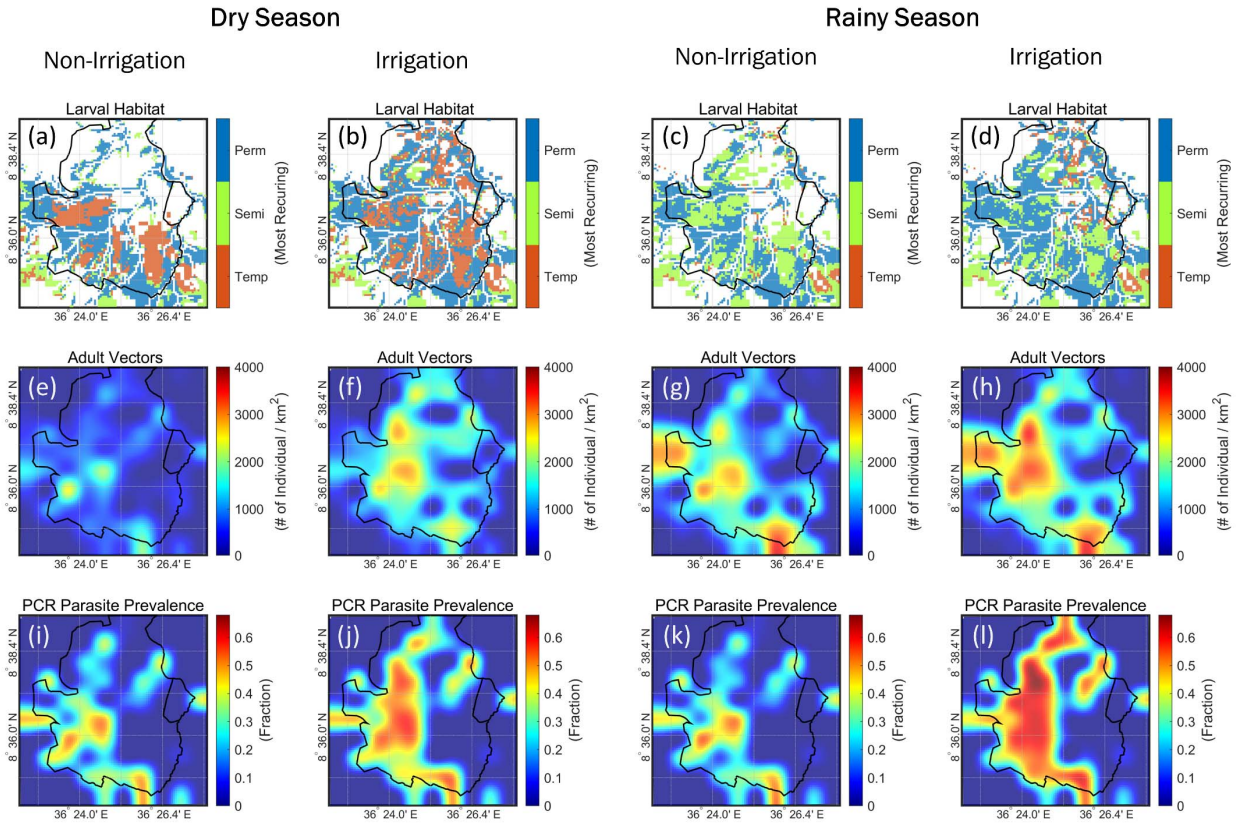

Figure 9. Spatial distribution of daily average larval habitats, adult vectors, and parasite prevalence diagnosed by Polymerase Chain Reaction (PCR) in the dry season (November 2016-April 2017) and the rainy season (May 2017-October 2017). This period was selected because the effect of irrigation on malaria transmission was the most pronounced. The simulated larval habitats, adult vectors, and PCR parasite prevalence from *Non-Irrigation* are presented in (a), (e) and (i) for the dry season and (c), (g) and (k) for the rainy season. Similarly, the simulated larval habitats, adult vectors and PCR parasite prevalence from *Irrigation* are presented in (b), (f) and

(j) for the dry season and (d), (h) and (l) for the rainy season. Their spatially averaged values can be found in Table S4.

4. Discussion

4.1. Role of Hydrology in Degree of Habitat Seasonality and Implications on Transmission

The average vector infection and prevalence rates in *Default EMOD* over the simulation period were significantly higher than *Integrated EMOD*. From Figure 5a, one of the most noticeable differences between the two scenarios was the degree of seasonality of the larval habitat. Although the mean habitat area was set the same in both scenarios, the magnitude of the seasonal variation was larger when hydrologic modeling was incorporated. This is mainly because the hydrologic model in *Integrated EMOD* considers complex physical processes and characteristics specific to the study area, including topography, land use, and soil. At the same time, *Default EMOD* adopts a parsimonious, one-size-fits-all approach. Specifically, the default habitat function in EMOD assumed that the permanent habitat area was at equilibrium and remained constant throughout the simulation. In reality, permanent habitats such as those on river edges can vary in the area with climate conditions. In addition, there was no infiltration mechanism for the other two habitat types (Equation (1) and Equation (3)), so new ponds started forming immediately at the onset of the rainy season and continued forming towards the end of the rainy season whenever there was rainfall. The result was an earlier rising limb and a delayed falling limb in the time series compared to *Integrated EMOD* (see Figure S13 for an example). As the mean area in both scenarios was the same, the *Default EMOD* time series naturally ended up with a broader but flatter crest.

Due to the high larval capacity for permanent habitats, the habitat larval capacity time series in *Default EMOD* becomes even more invariant (Figure S11c). Therefore, to evaluate the effect of the degree of seasonality in the larval habitat on malaria transmission, we conducted a sensitivity analysis using a synthetic sinusoidal time series for larval habitat fractional area with the same mean but different amplitudes:

$$F_{\alpha}^{t} = \alpha \cos(365.25t + 125.2) + \bar{F}, \tag{6}$$

where α is the amplitude of fractional area, F_{α}^{t} is the fractional area at time t, $\bar{F}$ is the mean fractional area specific to the study derived from the hydrologic model.

The sensitivity analysis results can be found in Figure S14 and are summarized in Table 2. By reducing the seasonal amplitude from 0.2 to 0.1, the adult vector population remained relatively unchanged, but the vector infection and prevalence rates tripled. For the extreme case when α was reduced to 0, the vector infection and prevalence rates increased further by 4.29 times and 4.80 times, respectively. This finding agrees with the higher simulated malaria transmission in *Default EMOD* compared to *Integrated EMOD* (Figure S11e-g). It is possible that in the case where α was 0, the consistent adult vector population arising from the invariant habitat availability resulted in a stable parasite transmission throughout the year. As α increased, the disparity between the high and low vector abundance seasons increased. In the low vector abundance season, the transmission was minimal. In the high vector abundance season, transmission increased but would be limited by the human population. This resulted in an overall lower annual average vector infection rate and prevalence. Therefore, a nuanced approach

considering the trend of the mean and the degree of the seasonality of larval habitats is required to predict malaria transmission accurately.

Table 2. Average simulated adult vector abundance, adult vector infection rate, and parasite prevalence rate for different amplitudes of larval habitat seasonality, α.

α	Adult Vectors	Vectors Infection Rate	Parasite Prevalence Rate
0.2	1.00	1.00	1.00
0.15	1.00	2.10	2.22
0.1	1.01	2.96	3.23
0.05	1.01	3.76	4.18
0	1.01	4.29	4.80

EMOD was designed primarily to model disease transmission and guide efforts toward malaria eradication. Vector ecology in simplified larval habitat equations is incorporated into the model with the primary goal of capturing transmission. Malaria studies that use EMOD adjust mosquito lifecycle parameters to match real-world transmission metrics, including, but not limited to, prevalence and incidence. In scenarios where field EIR data is readily available, the modeling of vector ecology may even be bypassed entirely. In the former, parameter calibration may not compensate for the simplified vector ecology representation in EMOD. In the latter, the approach is highly dependent on the availability of field data. By incorporating hydrologic modeling, we seek to improve the representation of larval habitats in EMOD as a first step toward a more robust simulation of malaria transmission. In the future, other mosquito lifecycle parameters that are seldom considered, such as mosquito emergence rates, should be calibrated. This requires field data beyond prevalence and incidence, such as habitat productivity and adult mosquito abundance.

4.2. Insights Provided by Modeling on the Effect of Irrigation

By coupling hydrologic modeling with EMOD, we were able to investigate the effect of irrigation on malaria by comparing two scenarios whereby irrigation was the only difference. This allows us to isolate the effect of other environmental and social variables, such as temperature, rainfall, topography, and demography, from the relationship between irrigation and malaria transmission. The significance of our approach is that it supplements past field comparative studies whereby the effect of irrigation could have been obscured by different field settings (Ijumba & Lindsay, 2001). The approach also has the potential to explore hypothetical scenarios to guide better decision-making in water resource management.

Our modeling elucidates a few ways in which irrigation affected malaria transmission dynamics through larval habitats. First, all three habitat types increased in the dry season, while temporary and semi-permanent habitats were converted to permanent habitats in the rainy season. During the dry season, permanent habitats were the predominant habitat without irrigation, but irrigation significantly increased the area of the temporary and semi-permanent habitats (Figure 7a). The result was an increased diversity of the habitats which agrees with field observations (Hawaria et al., 2019). On the other hand, permanent habitats became even more dominant in the rainy season with irrigation. The change in relative abundance and stability of the habitats may favor the growth and survival of one vector species over the other, shifting the

predominant vector species in the extreme case (Bamou et al., 2018; Chaves et al., 2021; Naranjo-Díaz et al., 2020).

Next, irrigation not only creates transmission all-year round but also intensifies the primary transmission period associated with the rainy season in terms of EIR and prevalence rate (Figure 8e-f). Studies have shown that irrigation can extend malaria transmission throughout the year due to water availability for breeding in the dry season (Kibret et al., 2014). Our results show that irrigation during the dry season can also increase the stability of the habitats in the rainy season by creating high soil moisture conditions favorable for ponding before the onset of the rainy season. As habitat stability is linked to adult vector density (Ndenga et al., 2011), this caused a more significant proliferation in adult vectors during the rainy season compared to *Non-Irrigation*. Besides a larger adult vector population in the rainy season, there could also be a carryover of parasites in the human population from the preceding dry season, resulting in a higher vector infection rate. This ripple effect has been observed in past studies investigating the link between malaria transmission season and preceding rainfall (Midekisa et al., 2015; Pascual et al., 2008). Our results suggest that irrigation can also produce the same cascading effect.

Thirdly, the modeling revealed that peak malaria transmission was shifted forward by around one month in the irrigation scenario (Figure 8e-f). Studies in East Africa have shown that rainfall significantly correlates with malaria transmission with a lag time of 1 to 2 months (Loevinsohn, 1994; Zhou et al., 2004). The lag can be attributed to the time for infiltration to occur, runoff to accumulate in low-lying areas, and the development time for parasite growth. In addition, past observations have proven that irrigation plays the same function as rainfall in providing larval habitats to support vector growth (Herrel et al., 2001; Ohta & Kaga, 2014). Hence, irrigation in the dry season in our study created a pseudo-early rainy season, which causes earlier onset of mosquito breeding and a peak in transmission.

Lastly, we demonstrated the effect of irrigation on the spatiotemporal distribution of malaria transmission by considering the heterogeneity of larval habitats (Figure 9). While past observations have told us that irrigation can increase the adult vector population (Demissew et al., 2020), it remains a challenge to predict where and when breeding will occur (Frake et al., 2020). Integrating local irrigation practices and environmental characteristics such as land use, topography, and soil properties, the model provided new insights into the breeding hotspots broken down into temporary, semi-permanent, and permanent habitat types. This information can help larval source management (LSM) as a supplementary vector control by prioritizing resources for operational planning. LSM is known to be efficient where habitats are findable, few and fixed (Djamouko-Djonkam et al., 2019; Stanton et al., 2021). Based on the results, we can identify the location of habitats, determine the period with manageable habitat abundance, and single out semi-permanent and permanent habitats for targeted larviciding. Comparing *Non-Irrigation* to *Irrigation* also allows us to distinguish habitats' hotspots induced by irrigation from those already present without irrigation. Other means, such as water resource management, can then be considered to control the former.

5. Conclusion

Malaria transmission is intrinsically related to larval habitats, which cannot be characterized by climate alone. By coupling a hydrologic model with an agent-based malaria model, the variability of larval habitats increased and resulted in significantly lower malaria transmission as opposed to modeling habitats based on a simplified function of climate factors.

We also demonstrated how habitat heterogeneity based on hydrologic processes could affect the spatiotemporal dynamics of malaria transmission.

The hydrology-integrated framework enabled us to investigate the effect of irrigation on malaria transmission through changes to larval habitats broken down into temporary, semi-permanent, and permanent types. The results indicated that all three habitat types increased in the dry season, while temporary and semi-permanent habitats were converted to permanent habitats during the rainy season. This influenced the transmission dynamics significantly as the transmission was sustained all-year round and intensified during the primary season. Lastly, the peak malaria transmission was found to be shifted forward by around one month. These insights can help guide malaria intervention strategies to mitigate the effect of irrigation.

The study presents a novel generalizable framework that simulates the spatiotemporal dynamics of malaria transmission under the influence of irrigation by integrating hydrologic modeling with an agent-based model. The framework is a first step toward developing tailor-made intervention strategies by simulating different water resource management practices. This is crucial to the continued implementation of irrigation schemes for food security while minimizing the impact on malaria transmission.

Acknowledgments

We thank the team from the FDRE Sugar Corporation Arjo-Didessa Sugar Factory (Ethiopia) for providing their valuable time for interviews and datasets for model development and validation. We also thank the support team from the Research Cyberinfrastructure Center at University of California Irvine for their help with the use of high performance computing facility. Lastly, we are grateful for the software and technological supports from Daniel Bridenbecker and the EMOD malaria team at the Institute for Disease Modeling of the Bill and Melinda Gates Foundation. This work was supported by grants from National Institutes of Health (U19 AI129326), U.S. Department of Energy (HydroWIRES Initiative DE-EE0008943) and California Department of Water Resources (AR Program 4600013361). The funders had no role in the study design, data collection, analysis, decision to publish, or preparation of the manuscript.

Conflict of Interest Statement

The authors declare no conflicts of interest relevant to this study.

Open Research

The simulation softwares used in this research, ParFlow-CLM and EMOD, are available at https://doi.org/10.5281/zenodo.4816884 and https://github.com/InstituteforDiseaseModeling/EMOD respectively. The precipitation records used as model input can be downloaded from the Data Portal at Center for Hydrometeorology & Remote Sensing (Nguyen et al., 2019). Other climate input data can be retrieved from Climate Data Store (Copernicus Climate Change Service, 2023). Surface elevation data from can be purchased using the website https://www.aw3d.jp/en/contactform/. Land cover data are available from http://www.globallandcover.com/home_en.html and soil data can be downloaded from the SoilGrid database (https://soilgrids.org/). The larval habitat and malaria incidence data used to calibrate EMOD are available from Zenodo (https://doi.org/10.5281/zenodo.7972323).

References

Asare, Ernest O., Tompkins, A. M., Amekudzi, L. K., & Ermert, V. (2016). A breeding site model for regional, dynamical malaria simulations evaluated using in situ temporary ponds observations. *Geospatial Health*, *11*(1S), 390. https://doi.org/10.4081/gh.2016.390

Asare, Ernest Ohene, Tompkins, A. M., & Bomblies, A. (2016). A Regional Model for Malaria Vector Developmental Habitats Evaluated Using Explicit, Pond-Resolving Surface Hydrology Simulations. *PLOS ONE*, *11*(3), e0150626. https://doi.org/10.1371/journal.pone.0150626

Ashby, S. F., & Falgout, R. D. (1996). A parallel multigrid preconditioned conjugate gradient algorithm for groundwater flow simulations. *Nuclear Science and Engineering*, *124*(1), 145–159. https://doi.org/10.13182/NSE96-A24230

Bamou, R., Mbakop, L. R., Kopya, E., Ndo, C., Awono-Ambene, P., Tchuinkam, T., et al. (2018). Changes in malaria vector bionomics and transmission patterns in the equatorial forest region of Cameroon between 2000 and 2017. *Parasites and Vectors*, *11*(1), 1–13. https://doi.org/10.1186/s13071-018-3049-4

Bill & Melinda Gates Foundation. (2022). Overview of EMOD software. Retrieved May 11, 2022, from https://docs.idmod.org/projects/emod-malaria/en/2.20_a/software-overview.html

Bomblies, A., Duchemin, J.-B., & Eltahir, E. A. B. (2008). Hydrology of malaria: Model development and application to a Sahelian village. *Water Resources Research*, *44*(12). https://doi.org/10.1029/2008WR006917

Chaves, L. S. M., Bergo, E. S., Conn, J. E., Laporta, G. Z., Prist, P. R., & Sallum, M. A. M. (2021). Anthropogenic landscape decreases mosquito biodiversity and drives malaria vector proliferation in the Amazon rainforest. *PLoS ONE*, *16*(1), e0245087. https://doi.org/10.1371/journal.pone.0245087

Chen, J., Chen, J., Liao, A., Cao, X., Chen, L., Chen, X., et al. (2015). Global land cover mapping at 30 m resolution: A POK-based operational approach. *ISPRS Journal of Photogrammetry and Remote Sensing*, *103*, 7–27. https://doi.org/10.1016/j.isprsjprs.2014.09.002

Copernicus Climate Change Service, C. D. S. (2023). ERA5 hourly data on single levels from 1940 to present. https://doi.org/10.24381/cds.adbb2d47

Cosgrove, B. A., Lohmann, D., Mitchell, K. E., Houser, P. R., Wood, E. F., Schaake, J. C., et al. (2003). Real-time

and retrospective forcing in the North American Land Data Assimilation System (NLDAS) project. *Journal of Geophysical Research: Atmospheres*, *108*(22). https://doi.org/10.1029/2002jd003118

Demissew, A., Hawaria, D., Kibret, S., Animut, A., Tsegaye, A., Lee, M. C., et al. (2020). Impact of sugarcane irrigation on malaria vector Anopheles mosquito fauna, abundance and seasonality in Arjo-Didessa, Ethiopia. *Malaria Journal*, *19*(1), 1–8. https://doi.org/10.1186/s12936-020-03416-0

Djamouko-Djonkam, L., Mounchili-Ndam, S., Kala-Chouakeu, N., Nana-Ndjangwo, S. M., Kopya, E., Sonhafouo-Chiana, N., et al. (2019). Spatial distribution of Anopheles gambiae sensu lato larvae in the urban environment of Yaoundé, Cameroon. *Infectious Diseases of Poverty*, *8*(1), 1–15. https://doi.org/10.1186/s40249-019-0597-6

Eckhoff, P. (2013). Mathematical models of within-host and transmission dynamics to determine effects of malaria interventions in a variety of transmission settings. *American Journal of Tropical Medicine and Hygiene*, *88*(5), 817–827. https://doi.org/10.4269/ajtmh.12-0007

Eckhoff, P. A. (2011). A malaria transmission-directed model of mosquito life cycle and ecology. *Malaria Journal*, *10*(1), 1–17. https://doi.org/10.1186/1475-2875-10-303

Fikadu, A. (2015). *Performance evaluation of sprinkler irrigation at Arjo Dedessa sugar development project, Oromia region*. Arba Minch Institute of Technology. https://doi.org/10.20372/nadre:1554185288.85

Frake, A. N., Namaona, W., Walker, E. D., & Messina, J. P. (2020). Estimating spatio-temporal distributions of mosquito breeding pools in irrigated agricultural schemes: A case study at the Bwanje Valley Irrigation Scheme. *Malaria Journal*, *19*(1), 1–21. https://doi.org/10.1186/s12936-020-3113-3

Galactionova, K., Smith, T. A., & Penny, M. A. (2021). Insights from modelling malaria vaccines for policy decisions: the focus on RTS,S. *Malaria Journal*, *20*(1), 1–8. https://doi.org/10.1186/s12936-021-03973-y

Gerardin, J., Ouédraogo, A. L., McCarthy, K. A., Eckhoff, P. A., & Wenger, E. A. (2015). Characterization of the infectious reservoir of malaria with an agent-based model calibrated to age-stratified parasite densities and infectiousness. *Malaria Journal*, *14*(1), 1–13. https://doi.org/10.1186/S12936-015-0751-Y

Gleeson, T., Moosdorf, N., Hartmann, J., & van Beek, L. P. H. (2014). A glimpse beneath earth's surface: GLobal HYdrogeology MaPS (GLHYMPS) of permeability and porosity. *Geophysical Research Letters*, *41*(11), 3891–3898. https://doi.org/10.1002/2014GL059856

Griffin, J. T., Hollingsworth, T. D., Okell, L. C., Churcher, T. S., White, M., Hinsley, W., et al. (2010). Reducing Plasmodium falciparum malaria transmission in Africa: A model-based evaluation of intervention strategies. *PLoS Medicine*, *7*(8), e1000324. https://doi.org/10.1371/journal.pmed.1000324

Haileselassie, W., Zemene, E., Lee, M. C., Zhong, D., Zhou, G., Taye, B., et al. (2021). The effect of irrigation on malaria vector bionomics and transmission intensity in western Ethiopia. *Parasites and Vectors*, *14*(1), 1–11. https://doi.org/10.1186/s13071-021-04993-y

Hardy, A. J., Gamarra, J. G. P., Cross, D. E., Macklin, M. G., Smith, M. W., Kihonda, J., et al. (2013). Habitat Hydrology and Geomorphology Control the Distribution of Malaria Vector Larvae in Rural Africa. *PLoS ONE*, *8*(12), e81931. https://doi.org/10.1371/journal.pone.0081931

Hartung, C., Lerer, A., Anokwa, Y., Tseng, C., Brunette, W., & Borriello, G. (2010). Open Data Kit: Tools to Build Information Services for Developing Regions. In *Proceedings of the 4th ACM/IEEE International Conference on Information and Communication Technologies and Development* (pp. 1–12). New York, United States: Association for Computing Machinery. https://doi.org/10.1145/2369220.2369236

Hawaria, D., Getachew, H., Zhong, G., Demissew, A., Habitamu, K., Raya, B., et al. (2019). Ten years malaria trend at Arjo-Didessa sugar development site and its vicinity, Southwest Ethiopia: A retrospective study. *Malaria Journal*, *18*(1), 1–11. https://doi.org/10.1186/s12936-019-2777-z

Hawaria, D., Demissew, A., Kibret, S., Lee, M. C., Yewhalaw, D., & Yan, G. (2020). Effects of environmental modification on the diversity and positivity of anopheline mosquito aquatic habitats at Arjo-Dedessa irrigation development site, Southwest Ethiopia. *Infectious Diseases of Poverty*, *9*(1), 1–11. https://doi.org/10.1186/s40249-019-0620-y

Hengl, T., Mendes de Jesus, J., Heuvelink, G. B. M., Ruiperez Gonzalez, M., Kilibarda, M., Blagotić, A., et al. (2017). SoilGrids250m: Global gridded soil information based on machine learning. *PLOS ONE*, *12*(2), e0169748. https://doi.org/10.1371/journal.pone.0169748

Herrel, N., Amerasinghe, F. P., Ensink, J., Mukhtar, M., Van Der Hoek, W., & Konradsen, F. (2001). Breeding of Anopheles mosquitoes in irrigated areas of South Punjab, Pakistan. *Medical and Veterinary Entomology*, *15*(3), 236–248. https://doi.org/10.1046/j.0269-283X.2001.00312.x

Hersbach, H., Bell, B., Berrisford, P., Biavati, G., Horányi, A., Muñoz Sabater, J., Nicolas, J., et al. (2018). ERA5 hourly data on single levels from 1959 to present. https://doi.org/10.24381/cds.adbb2d47

Ijumba, J. N., & Lindsay, S. W. (2001). Impact of irrigation on malaria in Africa: Paddies paradox. *Medical and*

Veterinary Entomology, *15*(1), 1–11. https://doi.org/10.1046/j.1365-2915.2001.00279.x

Jiang, A.-L., Lee, M.-C., Zhou, G., Zhong, D., Hawaria Dawit, Kibret, S., et al. (2021). Predicting Distribution of Malaria Vector Larval Habitats in Ethiopia by Integrating Distributed Hydrologic Modeling with Remotely Sensed Data. *Scientific Reports*, *11*(1), 1–14. https://doi.org/https://doi.org/10.1038/s41598-021-89576-8

Jiang, A.-L., Hsu, K., Sanders, B. F., & Sorooshian, S. (2023). Advances in Water Resources Topographic hydro-conditioning to resolve surface depression storage and ponding in a fully distributed hydrologic model. *Advances in Water Resources*, *176*(April), 104449. https://doi.org/10.1016/j.advwatres.2023.104449

Jones, J. E., & Woodward, C. S. (2001). Newton-Krylov-multigrid solvers for large-scale, highly heterogeneous, variably saturated flow problems. *Advances in Water Resources*, *24*(7), 763–774. https://doi.org/10.1016/S0309-1708(00)00075-0

Kibret, S., Wilson, G. G., Tekie, H., & Petros, B. (2014). Increased malaria transmission around irrigation schemes in Ethiopia and the potential of canal water management for malaria vector control. *Malaria Journal*, *13*(1), 1–12. https://doi.org/10.1186/1475-2875-13-360

Kollet, S. J., & Maxwell, R. M. (2006). Integrated surface–groundwater flow modeling: A free-surface overland flow boundary condition in a parallel groundwater flow model. *Advances in Water Resources*, *29*(7), 945–958. https://doi.org/10.1016/J.ADVWATRES.2005.08.006

Le, P. V. V., Kumar, P., & Ruiz, M. O. (2018). Stochastic lattice-based modelling of malaria dynamics. *Malaria Journal*, *17*(1), 1–17. https://doi.org/10.1186/s12936-018-2397-z

Loevinsohn, M. E. (1994). Climatic warming and increased malaria incidence in Rwanda. *The Lancet*, *343*(8899), 714–718. https://doi.org/10.1016/S0140-6736(94)91586-5

Mangani, C., Frake, A. N., Chipula, G., Mkwaila, W., Kakota, T., Mambo, I., et al. (2022). Proximity of Residence to Irrigation Determines Malaria Risk and Anopheles Abundance at an Irrigated Agroecosystem in Malawi. *American Journal of Tropical Medicine and Hygiene*, *106*(1), 283–292. https://doi.org/10.4269/ajtmh.21-0390

Maxwell, R. M. (2013). A terrain-following grid transform and preconditioner for parallel, large-scale, integrated hydrologic modeling. *Advances in Water Resources*, *53*, 109–117. https://doi.org/10.1016/J.ADVWATRES.2012.10.001

Maxwell, R. M., & Kollet, S. J. (2008). Interdependence of groundwater dynamics and land-energy feedbacks under climate change. *Nature Geoscience*, *1*(10), 665–669. https://doi.org/10.1038/ngeo315

Midekisa, A., Beyene, B., Mihretie, A., Bayabil, E., & Wimberly, M. C. (2015). Seasonal associations of climatic drivers and malaria in the highlands of Ethiopia. *Parasites and Vectors*, *8*(1), 1–11. https://doi.org/10.1186/s13071-015-0954-7

Montosi, E., Manzoni, S., Porporato, A., & Montanari, A. (2012). An ecohydrological model of malaria outbreaks. *Hydrology and Earth System Sciences*, *16*(8), 2759–2769. https://doi.org/10.5194/hess-16-2759-2012

Munga, S., Minakawa, N., Zhou, G., Mushinzimana, E., Barrack, O. O. J., Githeko, A. K., & Yan, G. (2006). Association between land cover and habitat productivity of malaria vectors in western Kenyan highlands. *American Journal of Tropical Medicine and Hygiene*, *74*(1), 69–75. https://doi.org/10.4269/ajtmh.2006.74.69

Naranjo-Díaz, N., Hernandez-Valencia, J. C., Marín, A., & Correa, M. M. (2020). Relationship between land cover and Anophelinae species abundance, composition and diversity in NW Colombia. *Infection, Genetics and Evolution*, *78*, 104114. https://doi.org/10.1016/j.meegid.2019.104114

Ndenga, B. A., Simbauni, J. A., Mbugi, J. P., Githeko, A. K., & Fillinger, U. (2011). Productivity of malaria vectors from different habitat types in the western kenya highlands. *PLoS ONE*, *6*(4), e19473. https://doi.org/10.1371/journal.pone.0019473

Nguyen, P., Shearer, E. J., Tran, H., Ombadi, M., Hayatbini, N., Palacios, T., et al. (2019). The CHRS data portal, an easily accessible public repository for PERSIANN global satellite precipitation data. *Scientific Data*, *6*(1), 1–10. https://doi.org/10.1038/sdata.2018.296

Ohta, S., & Kaga, T. (2014). Effect of irrigation systems on temporal distribution of malaria vectors in semi-arid regions. *International Journal of Biometeorology*, *58*(3), 349–359. https://doi.org/10.1007/s00484-012-0630-y

Ondeto, B. M., Wang, X., Atieli, H., Orondo, P. W., Ochwedo, K. O., Omondi, C. J., et al. (2022). Malaria vector bionomics and transmission in irrigated and non-irrigated sites in western Kenya. *Parasitology Research*, 1–17. https://doi.org/10.1007/s00436-022-07678-2

Orondo, P. W., Wang, X., Lee, M. C., Nyanjom, S. G., Atieli, H., Ondeto, B. M., et al. (2023). Habitat Diversity, Stability, and Productivity of Malaria Vectors in Irrigated and Nonirrigated Ecosystems in Western Kenya. *Journal of Medical Entomology*, *60*(1), 202–212. https://doi.org/10.1093/jme/tjac168

Parham, P. E., Pople, D., Christiansen-Jucht, C., Lindsay, S., Hinsley, W., & Michael, E. (2012). Modeling the role of environmental variables on the population dynamics of the malaria vector Anopheles gambiae sensu stricto. *Malaria Journal*, *11*(1), 1–13. https://doi.org/10.1186/1475-2875-11-271

Pascual, M., Cazelles, B., Bouma, M. J., Chaves, L. F., & Koelle, K. (2008). Shifting patterns: Malaria dynamics and rainfall variability in an African highland. *Proceedings of the Royal Society B: Biological Sciences*, *275*(1631), 123–132. https://doi.org/10.1098/rspb.2007.1068

Patz, J. A., Strzepek, K., Lele, S., Hedden, M., Greene, S., Noden, B., et al. (1998). Predicting key malaria transmission factors, biting and entomological inoculation rates, using modelled soil moisture in Kenya. *Tropical Medicine and International Health*, *3*(10), 818–827. https://doi.org/10.1046/j.1365-3156.1998.00309.x

Reiner, R. C., Perkins, T. A., Barker, C. M., Niu, T., Chaves, L. F., Ellis, A. M., et al. (2013). A systematic review of mathematical models of mosquito-borne pathogen transmission: 1970-2010. *Journal of the Royal Society Interface*, *10*(81). https://doi.org/10.1098/rsif.2012.0921

Ross, R. (1908). *Report on the Prevention of Malaria in Mauritius*. *Waterlow & Sons Ltd*. London. Retrieved from https://wellcomecollection.org/works/rjj6m9qm

Sadeghi, M., Nguyen, P., Naeini, M. R., Hsu, K., Braithwaite, D., & Sorooshian, S. (2021). PERSIANN-CCS-CDR, a 3-hourly 0.04° global precipitation climate data record for heavy precipitation studies. *Scientific Data*, *8*(1), 1–11. https://doi.org/10.1038/s41597-021-00940-9

Selvaraj, P., Wenger, E. A., & Gerardin, J. (2018). Seasonality and heterogeneity of malaria transmission determine success of interventions in high-endemic settings: a modeling study. *BMC Infectious Diseases*, *18*(1), 1–14. https://doi.org/10.1186/S12879-018-3319-Y

Smith, M. W., Macklin, M. G., & Thomas, C. J. (2013). Hydrological and geomorphological controls of malaria transmission. *Earth-Science Reviews*, *116*(1), 109–127. https://doi.org/10.1016/j.earscirev.2012.11.004

Smith, M. W., Willis, T., Alfieri, L., James, W. H. M., Trigg, M. A., Yamazaki, D., et al. (2020). Incorporating hydrology into climate suitability models changes projections of malaria transmission in Africa. *Nature Communications*, *11*(1), 1–9. https://doi.org/10.1038/s41467-020-18239-5

Smith, N. R., Trauer, J. M., Gambhir, M., Richards, J. S., Maude, R. J., Keith, J. M., & Flegg, J. A. (2018). Agent-based models of malaria transmission: A systematic review. *Malaria Journal*, *17*(1), 1–16. https://doi.org/10.1186/s12936-018-2442-y

Smith, T., Killeen, G. F., Maire, N., Ross, A., Molineaux, L., Tediosi, F., et al. (2006). Mathematical modeling of the impact of malaria vaccines on the clinical epidemiology and natural history of Plasmodium falciparum malaria: Overview. *The American Journal of Tropical Medicine and Hygiene*, *75*(Suppl 2), 1–10.

Stanton, M. C., Kalonde, P., Zembere, K., Hoek Spaans, R., & Jones, C. M. (2021). The application of drones for mosquito larval habitat identification in rural environments: a practical approach for malaria control? *Malaria Journal*, *20*(1), 1–17. https://doi.org/10.1186/s12936-021-03759-2

Takaku, J., & Tadono, T. (2017). Quality updates of 'AW3D' global DSM generated from ALOS PRISM. In *2017 IEEE International Geoscience and Remote Sensing Symposium (IGARSS)* (pp. 5666–5669). IEEE. https://doi.org/10.1109/IGARSS.2017.8128293

Ward, C., Torquebiau, R., & Xie, H. (2016). *Improved Agricultural Water Management for Africa's Drylands*. *World Bank Publications*. https://doi.org/10.1596/978-1-4648-0832-6

World Health Organization. (2021). *Word Malaria Report 2021*. Geneva, Switzerland.

Zhou, G., Minakawa, N., Githeko, A. K., & Yan, G. (2004). Association between climate variability and malaria epidemics in the East African highlands. *Proceedings of the National Academy of Sciences of the United States of America*, *101*(8), 2375–2380. https://doi.org/10.1073/pnas.0308714100

GeoHealth

Supporting Information for

Investigating the Impact of Irrigation on Malaria Larval Habitats and Transmission Using a Hydrology-based Model

Ai-Ling Jiang[1], Ming-Chieh Lee[2], Prashanth Selvaraj[3], Teshome Degefa[4, 5], Hallelujah Getachew[4,5,6], Hailu Merga[7], Delenasaw Yewhalaw[4,5], Guiyun Yan[2], Kuolin Hsu[1]

[1] Center for Hydrometeorology and Remote Sensing, Department of Civil and Environmental Engineering, University of California Irvine, Irvine, CA, USA

[2] Department of Population Health and Disease Prevention, School of Public Health, Susan and Henry Samueli College of Health Sciences, University of California Irvine, Irvine, CA, USA

[3] Institute for Disease Modeling, Bill and Melinda Gates Foundation, Seattle, WA, USA

[4] School of Medical Laboratory Sciences, Institute of Health, Jimma University, Jimma, Ethiopia

[5] Tropical and Infectious Diseases Research Center (TIDRC), Jimma University, Jimma, Ethiopia

[6] Department of Medical Laboratory Technology, Arbaminch College of Health Sciences, Arba Minch, Ethiopia

[7] Department of Epidemiology, Institute of Health, Jimma University, Jimma, Ethiopia

Contents of this file

Introduction

This file contains additional information on data collection, model development, calibration and simulation results.

Text S1. Larval density estimation

In the study area, the surveyed larval habitats include drainage ditch, river edge/reservoir shoreline, swamp/marsh, rice puddle, animal footprint, tire track/road puddle, man-made pond, natural pond/rain pool, rock pool, water container, irrigation canal, and brick pit. The larval habitats were classified as temporary, semi-permanent, or permanent based on their natural characteristics. Since larval density can be significantly different in the dry and rainy seasons (Hinne et al., 2021; Kweka et al., 2012) and the timing and duration of the survey periods were inconsistent, we sorted the measured larval densities from the 769 sample points (Figure 1) into the dry season (January to April; November to December) and the rainy season (May to October). We then calculated the average larval density for each season as shown in Figure S4.

In the surveyed area, the larval density for temporary habitats was higher in the rainy season than in the dry season during which the habitats are less stable. On the other hand, the larval densities for semi-permanent and permanent habitats were higher in the dry season. Most of the semi-permanent and permanent habitats were associated with river edges and swamps, whereby the larvae are prone to flushing in the rainy season. Finally, the larval density in Table 1 was calculated based on the average dry season and rainy season densities.

Text S2. Irrigation schedule design

Figure S6 shows the monthly irrigation schedule obtained from the Arjo-Didessa Sugar Factory, which is tailored to the sugarcane planting cycle.

To model irrigation in ParFlow-CLM, the irrigation interval and rate are required user inputs. A report provided by the factory recommended 8-12 days for the design of the local irrigation system, so we set the irrigation interval as 10 days.

To determine the irrigation rate, we first calculated the irrigation depth, defined as the amount of water that needs to be applied when the soil water content is depleted to the wilting point. The irrigation depth ($IrrD$) was calculated as

$$IrrD = (FC - WP) \times Depth_{soil}, \tag{S1}$$

where FC is the field capacity, WP is the permanent wilting point and $Depth_{soil}$ is the soil depth.

The study area is characterized by clay and clay loam with low permeability. Based on resources by the Northeast Region Certified Crop Advisor (https://nrcca.cals.cornell.edu/soil/CA2/CA0212.1-3.php), the field capacity volumetric soil moisture content of clay was set as 50%, and the wilting point volumetric soil moisture content was set as 15%. A soil depth of 2 m was assumed. Using Equation (S1), an irrigation depth of 700 mm was obtained.

We configured the irrigation to be applied when 50% of the irrigation depth was depleted; hence, the actual irrigation depth to be applied over the 10-day irrigation interval was 350 mm. Adopting an intermittent irrigation strategy, we set the irrigation to be applied for 22 hours a day over 3 days within the 10-day cycle. The irrigation rate was then calculated to be 5.3 mm/hour.

Text S3. Model calibration

At each grid cell, ponding is assumed to occur if the soil saturation exceeds the threshold, θ. Therefore, the threshold was calibrated to ensure that the model will predict the occurrence of ponding at locations in line with the field-surveyed larval habitats for soil saturation above θ. The value for θ was obtained based on a sensitivity analysis by altering the threshold and noting the corresponding change in the probability of detection (POD). The POD determines if the model can predict an aquatic habitat successfully and can be calculated based on the ratio of the number of successful predictions or hits, H, to the total number of samples, S:

$$POD = H/S, \tag{S2}$$

Figure S8 shows the results of the sensitivity analysis. Generally, the POD curve is higher for the simulation excluding dry season. This is because irrigation was only approximated by a simplified scheme in the dry season and may not reflect the localized irrigation dynamics. As the threshold was lowered, POD increased because ponding occurred across a larger area in the model. The influence of topography on the ponding was weakened, and the soil type became the dominant factor. On the other hand, when the threshold was increased, less ponding was predicted, resulting in a lower POD but the topographic variability was better represented. Therefore, we selected a threshold of 0.75 for a reasonable POD of 0.66 (excluding dry season) without obscuring topographic variability.

In EMOD, we calibrated 15 key parameters identified from a preliminary sensitivity analysis, and Table S3 presents the calibrated values. Using the calibrated parameters, we compared the simulated prevalence rate against field data for January 2018 and October 2018 (Figure S9). The results are within the same order of magnitude. In addition, we compared the simulated monthly number of clinical cases with the recorded malaria cases from April 2018 to May 2020 (Figure S10). Apart from the two peaks missed in October 2018 and November 2019, the simulated malaria cases compare reasonably well with observation in terms of magnitude and pattern. As the clinical malaria cases were sourced from major hospitals within the study area, the two peaks in recorded cases could be anomalous due to an influx of patients from outside seeking treatment at the hospitals. Overall, the model shows a good agreement with the field observation.

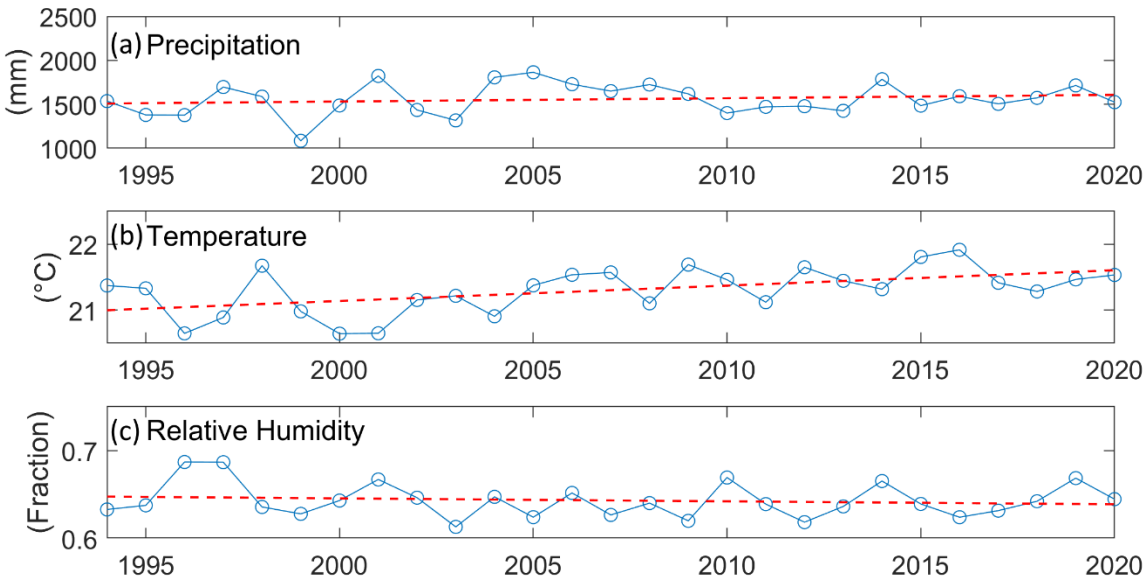

Figure S1. Annual climate data from PERSIANN-CCS-CDR and ERA5 for the study area. (a) total precipitation, (b) average temperature and (c) average relative humidity. The red dashed line represents the linear trendline in each subplot.

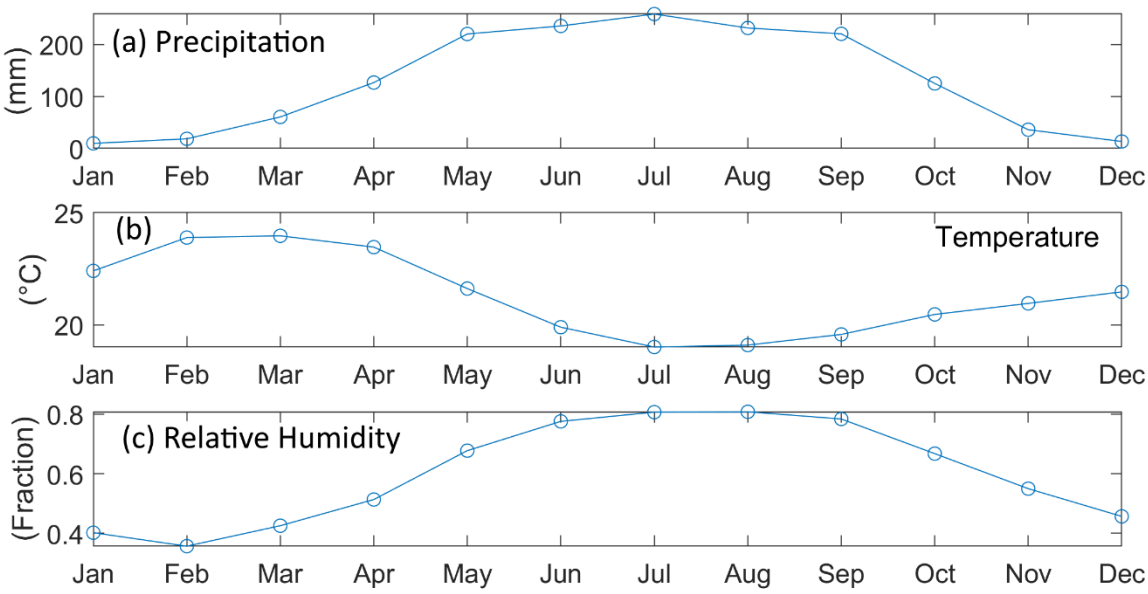

Figure S2. Monthly climate data (averaged from 1994 to 2020) derived from PERSIANN-CCS-CDR and ERA5 climate data for the study area. (a) total precipitation, (b) average temperature, and (c) average relative humidity.

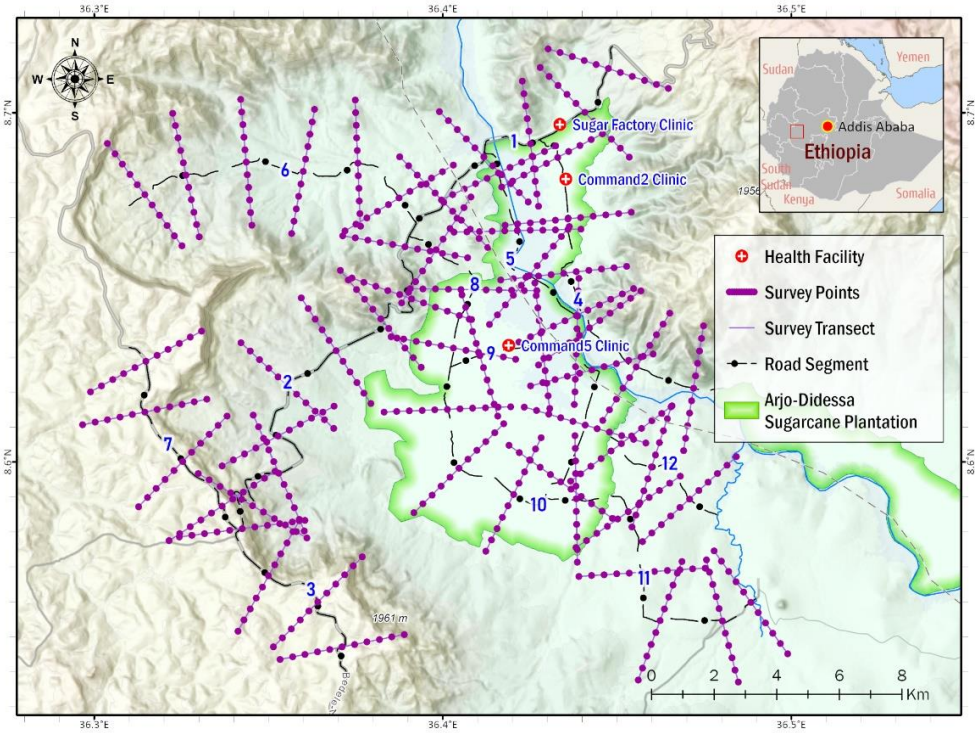

Figure S3. Land use survey locations.

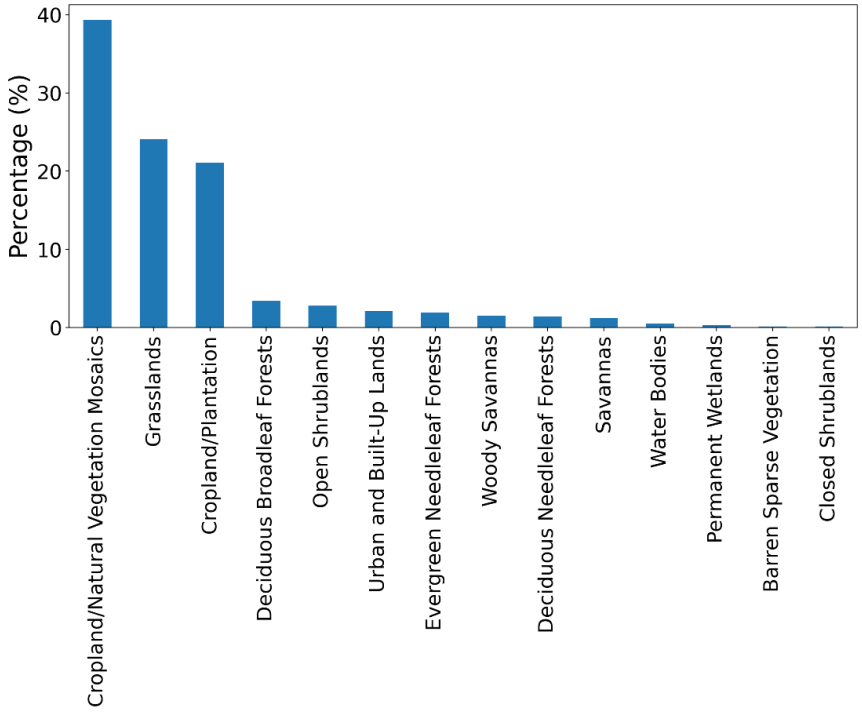

Figure S4. Percentage distribution of International Geosphere-Biosphere Programme type from land use survey.

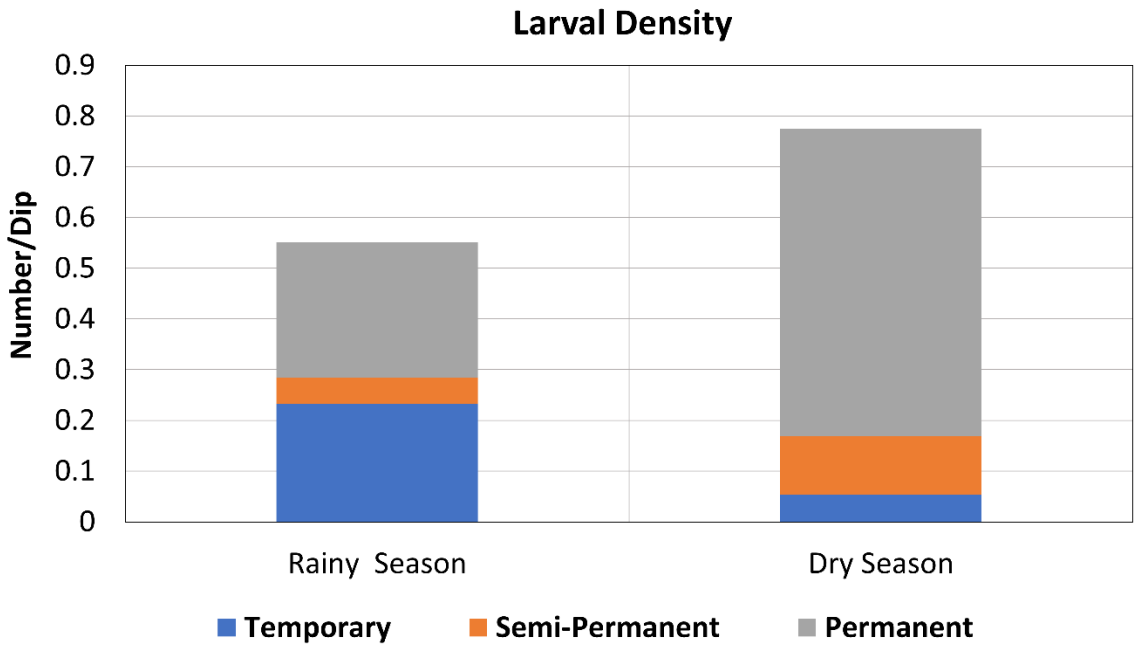

Figure S5. Average larval densities for temporary, semi-permanent, and permanent habitats during rainy and dry seasons from field survey.

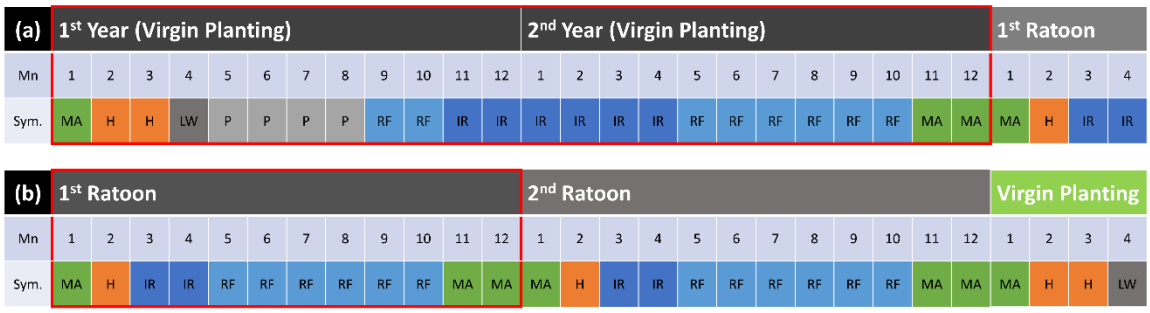

Figure S6. Arjo-Didessa Sugar Factory sugarcane plantation irrigation schedule. A typical sugar planting schedule includes (a) a 2-year cycle for virgin planting and (b) a 1-year cycle for the following 2 ratoons. MA: Maturity/water drain; H: Harvesting; LW: Land work; P: Planting; RF: Rainfed; IR: Irrigation.

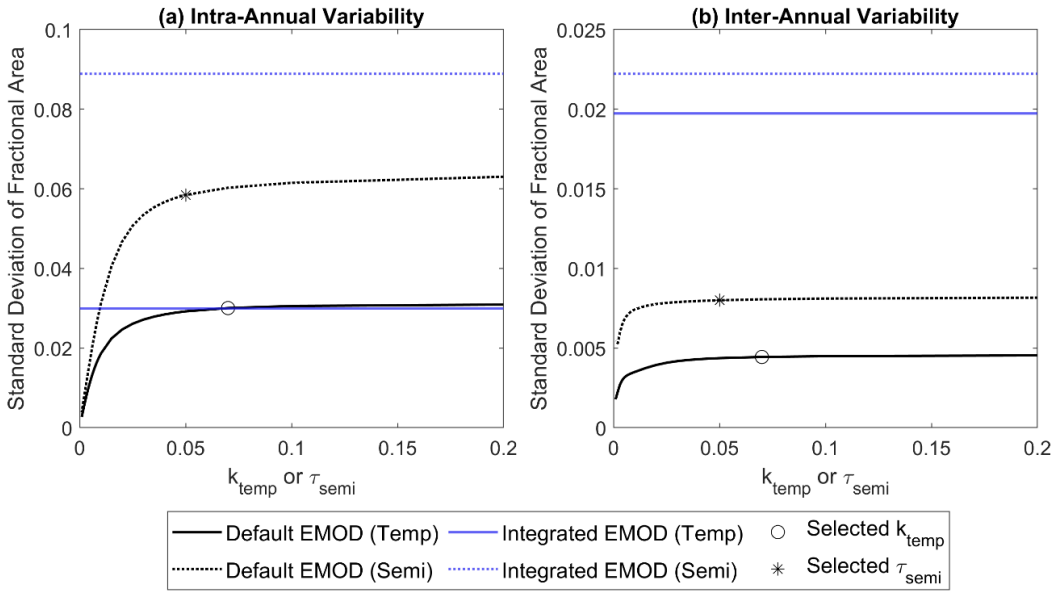

Figure S7. Adjustment of decay factors for temporary and semi-permanent habitats in default EMOD function. The objective was to match the (a) intra-annual variability and (b) inter-annual variability of the habitats from the hydrologic model as closely as possible. The decay factor of semi-permanent habitat also had to be smaller than that of temporary habitat. Intra-annual variability was measured in terms of the standard deviation of the 20-year average habitat area for each day of the year. Inter-annual variability was characterized by the standard deviation of the annual average habitat area for each year.

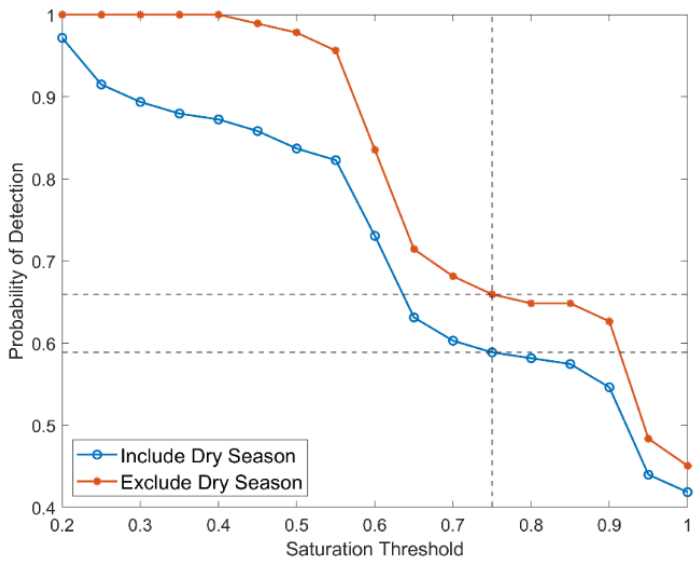

Figure S8. Sensitivity analysis of the probability of detection to saturation threshold. The probability of detection determines if the model can predict an aquatic habitat successfully and can be calculated based on the ratio of successful predictions to the total number of observations. The dotted vertical line corresponds to the selected threshold of 0.75, which

results in a reasonable POD of 0.66 excluding dry season and a POD of 0.59 including dry season.

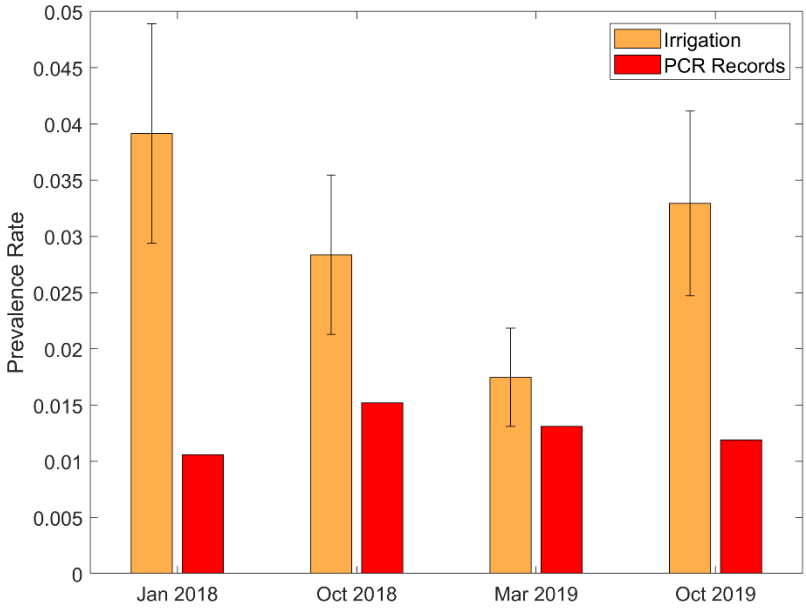

Figure S9. Comparison of simulated monthly average prevalence rate in *Irrigation* and measured prevalence diagnosed by Polymerase Chain Reaction (PCR). The whisker on the bar plot represents one standard error.

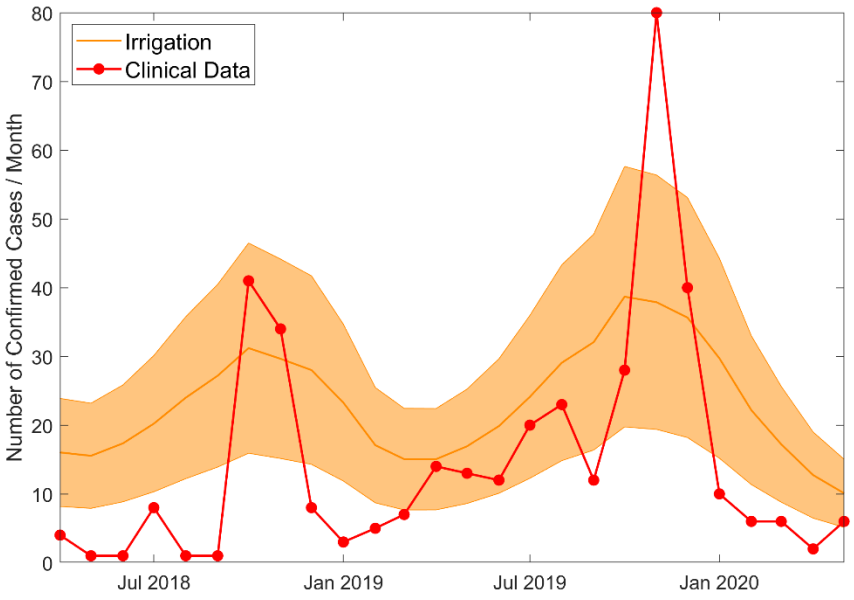

Figure S10. Comparison of simulated monthly confirmed cases in *Irrigation* and clinical data. The orange band indicates the 95% confidence interval.

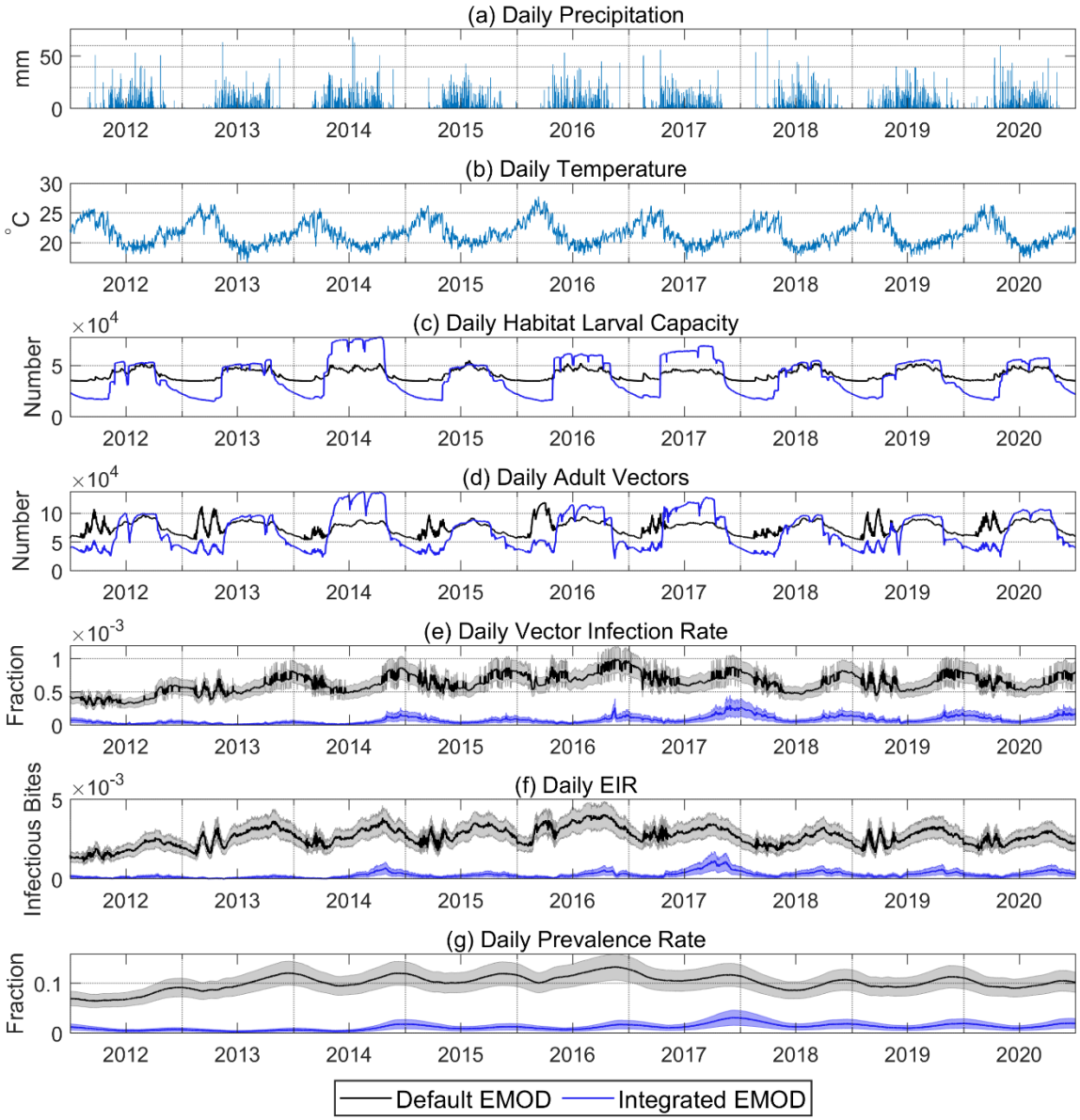

Figure S11. Time series of daily climate data and comparison of simulated daily malaria transmission results between *Default EMOD* and *Integrated EMOD*. Climate data include (a) precipitation and (b) temperature. Malaria transmission results include (c) habitat larval capacity, (d) adult vector abundance, (e) adult vector infection rate, (f) entomological inoculation rate and (g) parasite prevalence rate. The simulation was performed for 20 years from 2000 to 2020, but here we only show the results from 2010 to 2020 for simplicity.

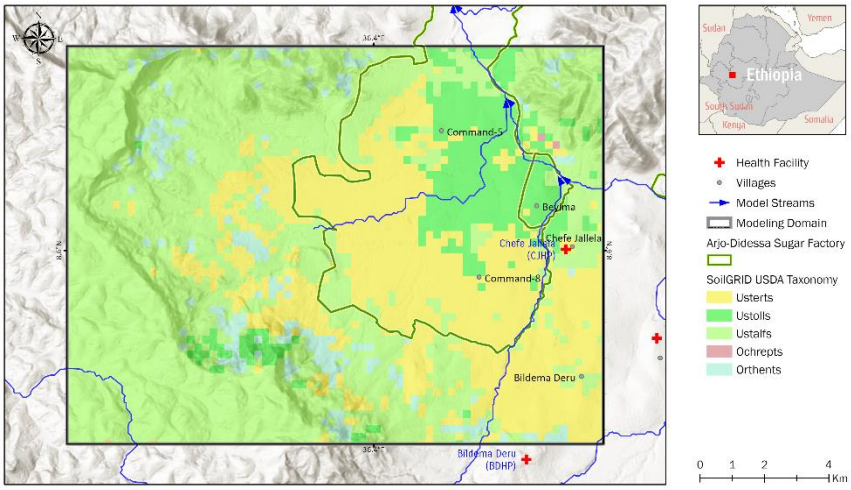

Figure S12. The distribution of the top two-meter soil types in USDA soil taxonomy from SoilGrids250m TAXOUSDA dataset. Most soil types in this area are characterized as clay or clay loam with low permeability ranging from 0.0015 to 0.015 m/h.

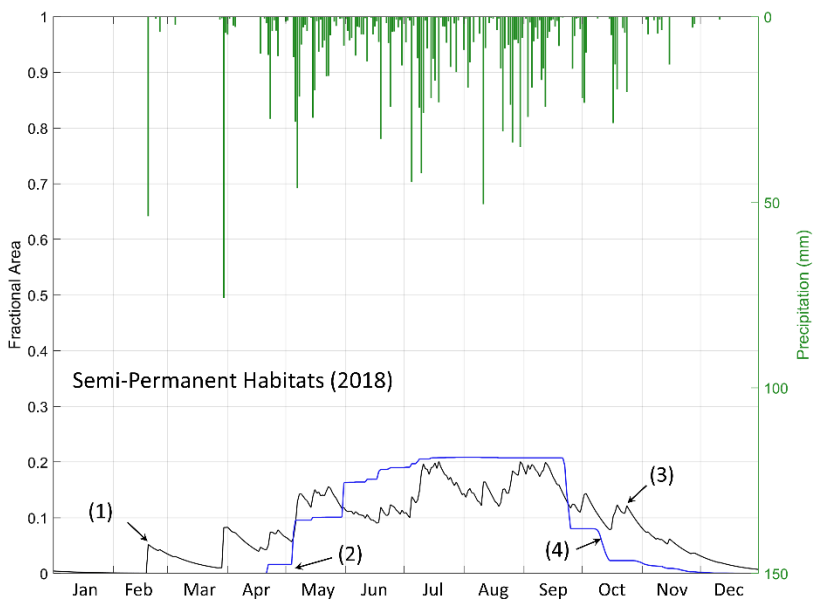

Figure S13. Comparison of simulated semi-permanent habitats between *Default EMOD* (black line) and *Integrated EMOD* (blue line) in 2018. Earlier rising limb in *Default EMOD*: (1) no infiltration, new ponds created instantaneously by rainfall; (2) ponds formed sometime after rainfall when soil saturation exceeded the threshold. Delayed falling limb in *Default EMOD*: (3) habitat area continued to increase with rainfall; (4) pond drained/dried up and soil became unsaturated after a period without rainfall, new rainfall insufficient to create ponding as soil saturation remained below threshold.

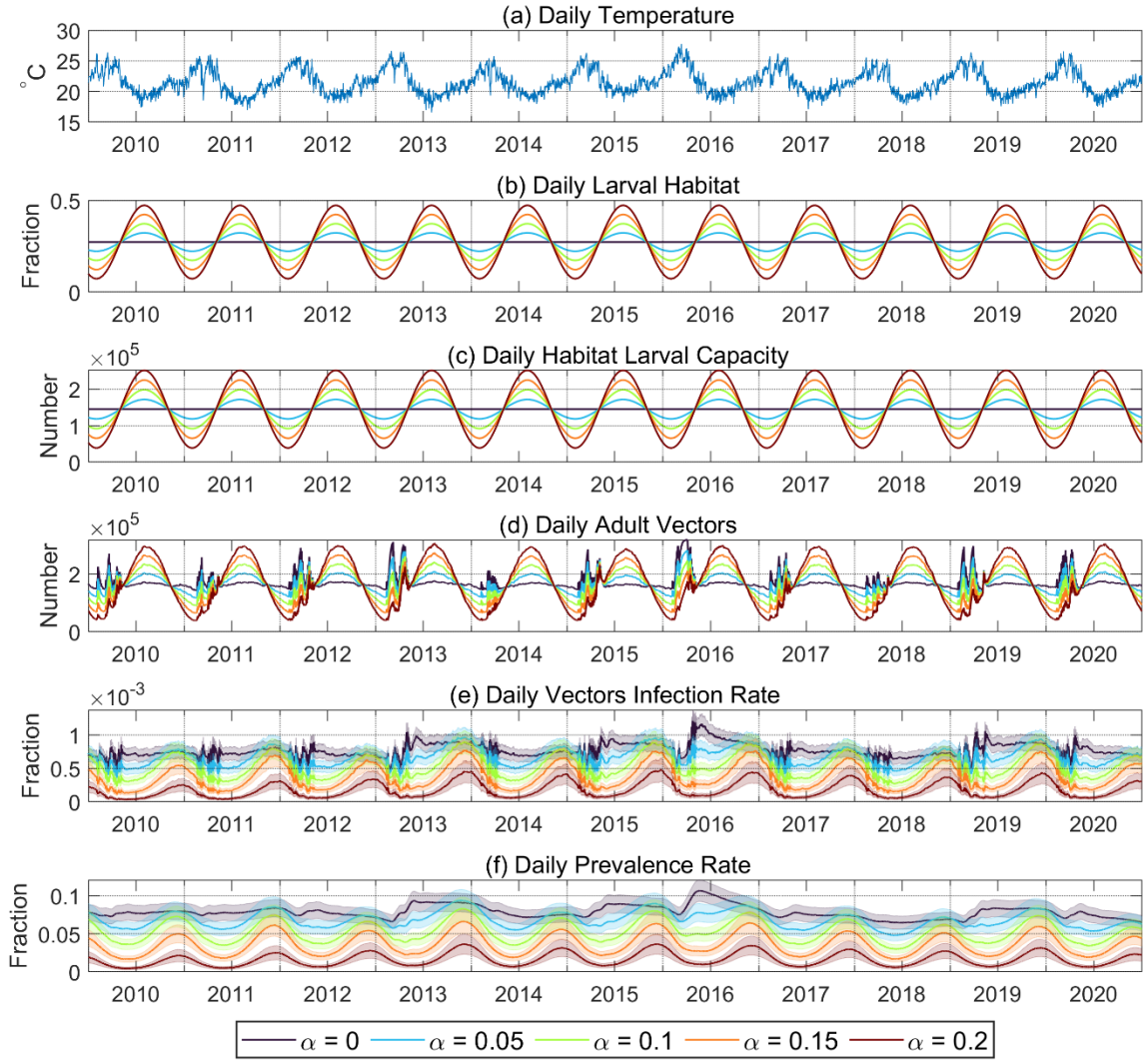

Figure S14. Simulation results from sensitivity analysis of malaria transmission to different amplitudes of larval habitat seasonality, $\boldsymbol{\alpha}$. Time series include (a) daily temperature, (b) synthetic sinusoidal larval habitat, (c) habitat larval capacity, (d) adult vector abundance, (e) adult vector infection rate and (f) parasite prevalence rate.

Table S1. Input data for ParFlow-CLM and EMOD.

Variable	Resolution	Latency	Source
Topography	5-meter	-	ALOS WORLD 3D Topographic Data (Takaku et al., 2016; Takaku and Tadono, 2017)
Precipitation	0.04°×0.04°, 3-hourly	~1 hour	Precipitation Estimation from Remotely Sensed Information using Artificial Neural Networks -Cloud Classification System- Climate Data Record (PERSIANN-CCS-CDR) (Sadeghi et al., 2021)
Surface Solar Radiation Downwards	0.25°×0.25°, 1-hourly	5 days	The Fifth Generation European Centre for Medium-Range Weather Forecasts Reanalysis (ERA5) (Hersbach et al., 2020, 2018)
Surface Thermal Radiation Downwards	0.25°×0.25°, 1-hourly	5 days	ERA5
Air Temperature (2m above ground surface)	0.25°×0.25°, 1-hourly	5 days	ERA5
Skin Temperature	0.25°×0.25°, 1-hourly	5 days	ERA5
Surface Pressure	0.25°×0.25°, 1-hourly	5 days	ERA5
Water-vapor specific humidity	0.25°×0.25°, 1-hourly	5 days	ERA5
North-to-South Component of Wind Speed (10m above ground surface)	0.25°×0.25°, 1-hourly	5 days	ERA5
East-to-West Component of Wind Speed (10m above ground surface)	0.25°×0.25°, 1-hourly	5 days	ERA5
Land Use (2000)	30-meter	-	Global Land Cover Mapping Project (GlobeLand30) (Chen et al., 2015)
Land Use (2010)	30-meter	-	GlobeLand30
Land Use (2020)	30-meter	-	GlobeLand30

Soil Type	250-meter	-	SoilGrids250m, TAXOUSDA (Hengl et al., 2017)
Depth to Bedrock	250-meter	-	SoilGrids250m, BDRICM (Hengl et al., 2017)
Near Surface Permeability (< 100 m)	Regional Scale	-	GLobal HYdrogeology MaPS 2.0 (GLHYMPS, 2.0) (Gleeson et al., 2014)

Table S2. Field data for ParFlow-CLM and EMOD validation.

Variable	Period	Number of Samples	Source
Land Use	July 2021	578	Site survey
Larval Habitat	2017-2021	769	Site survey
Population	2018-2021	-	Site survey
Prevalence Rate	January, October 2018; March, October 2019	4	Site survey
Clinical Case	April 2018-May 2020	26	Site survey

Table S3. Calibrated parameters in EMOD.

Parameter	Value
Antibody Memory Level	0.298
Base Sporozoite Survival Fraction	0.1667
Cytokine Gametocyte Inactivation	0.01335
Falciparum PfEMP1 Variants	150
Mean Sporozoites Per Bite	6
Merozoites Per Hepatocyte	990
Min Adapted Response	0.0174
Pyrogenic Threshold	500
Adult Life Expectancy	20
Male Life Expectancy	14
Aquatic Arrhenius 1	85,884,000,000

Aquatic Arrhenius 2	7,495
Infected Arrhenius 1	119,340,000,000
Infected Arrhenius 2	7,502
Scaling factor for larval capacity	1.66×10^{-5}

Table S4. Spatial average of adult vector and parasite prevalence rate from the dry season (November 2016 to April 2017) and the rainy season (May 2017 to October 2017).

Scenario	Dry Season		Rainy Season	
	Adult Vectors (# /km^2)	**Prevalence** (Fraction)	**Adult Vectors** (# /km^2)	**Prevalence** (Fraction)
Default EMOD	697	0.120	800	0.108
Integrated EMOD (Non-Irrigation)	451	0.111	961	0.107
Irrigation	889	0.154	1,140	0.182

References

Chen, Jun, Chen, Jin, Liao, A., Cao, X., Chen, L., Chen, X., He, C., Han, G., Peng, S., Lu, M., Zhang, W., Tong, X., Mills, J., 2015. Global land cover mapping at 30 m resolution: A POK-based operational approach. ISPRS J. Photogramm. Remote Sens. 103, 7–27. https://doi.org/10.1016/j.isprsjprs.2014.09.002

Gleeson, T., Moosdorf, N., Hartmann, J., van Beek, L.P.H., 2014. A glimpse beneath earth's surface: GLobal HYdrogeology MaPS (GLHYMPS) of permeability and porosity. Geophys. Res. Lett. 41, 3891–3898. https://doi.org/10.1002/2014GL059856

Hengl, T., Mendes de Jesus, J., Heuvelink, G.B.M., Ruiperez Gonzalez, M., Kilibarda, M., Blagotić, A., Shangguan, W., Wright, M.N., Geng, X., Bauer-Marschallinger, B., Guevara, M.A., Vargas, R., MacMillan, R.A., Batjes, N.H., Leenaars, J.G.B., Ribeiro, E., Wheeler, I., Mantel, S., Kempen, B., 2017. SoilGrids250m: Global gridded soil information based on machine learning. PLoS One 12, e0169748. https://doi.org/10.1371/journal.pone.0169748

Hersbach, H., Bell, B., Berrisford, P., Biavati, G., Horányi, A., Muñoz Sabater, J., Nicolas, J., Peubey, C., Radu, R., Rozum, I., Schepers, D., Simmons, A., Soci, C., Dee, D., Thépaut, J.-N., 2018. ERA5 hourly data on single levels from 1959 to present [WWW Document]. Copernicus Clim. Chang. Serv. Clim. Data Store. https://doi.org/10.24381/cds.adbb2d47

Hersbach, H., Bell, B., Berrisford, P., Hirahara, S., Horányi, A., Muñoz-Sabater, J., Nicolas, J., Peubey, C., Radu, R., Schepers, D., Simmons, A., Soci, C., Abdalla, S., Abellan, X., Balsamo, G., Bechtold, P., Biavati, G., Bidlot, J., Bonavita, M., De Chiara, G., Dahlgren, P., Dee, D., Diamantakis, M., Dragani, R., Flemming, J., Forbes, R., Fuentes, M., Geer, A., Haimberger, L.,

Healy, S., Hogan, R.J., Hólm, E., Janisková, M., Keeley, S., Laloyaux, P., Lopez, P., Lupu, C., Radnoti, G., de Rosnay, P., Rozum, I., Vamborg, F., Villaume, S., Thépaut, J.N., 2020. The ERA5 global reanalysis. Q. J. R. Meteorol. Soc. 146, 1999–2049. https://doi.org/10.1002/qj.3803

Hinne, I.A., Attah, S.K., Mensah, B.A., Forson, A.O., Afrane, Y.A., 2021. Larval habitat diversity and Anopheles mosquito species distribution in different ecological zones in Ghana. Parasites and Vectors 14, 1–14. https://doi.org/10.1186/s13071-021-04701-w

Kweka, E.J., Zhou, G., Munga, S., Lee, M.C., Atieli, H.E., Nyindo, M., Githeko, A.K., Yan, G., 2012. Anopheline Larval Habitats Seasonality and Species Distribution: A Prerequisite for Effective Targeted Larval Habitats Control Programmes. PLoS One 7, e52084. https://doi.org/10.1371/journal.pone.0052084

Sadeghi, M., Nguyen, P., Naeini, M.R., Hsu, K., Braithwaite, D., Sorooshian, S., 2021. PERSIANN-CCS-CDR, a 3-hourly 0.04° global precipitation climate data record for heavy precipitation studies. Sci. Data 8, 1–11. https://doi.org/10.1038/s41597-021-00940-9

Takaku, J., Tadono, T., 2017. Quality updates of 'AW3D' global DSM generated from ALOS PRISM, in: 2017 IEEE International Geoscience and Remote Sensing Symposium (IGARSS). IEEE, pp. 5666–5669. https://doi.org/10.1109/IGARSS.2017.8128293

Takaku, J., Tadono, T., Tsutsui, K., Ichikawa, M., 2016. Validation of 'AW3D' Global DSM Generated from ALOS PRISM. ISPRS Ann. Photogramm. Remote Sens. Spat. Inf. Sci. III–4, 25–31. https://doi.org/10.5194/isprsannals-III-4-25-2016